Testing and improving OMI DOMINO tropospheric NO$_2$ using observations from the DANDELIONS and INTEX-B validation campaigns

Jennifer C. Hains,[1,2] K. Folkert Boersma,[1] Mark Kroon,[1] Ruud J. Dirksen,[1]
Ronald C. Cohen,[3] Anne E. Perring,[3] Eric Bucsela,[4] Hester Volten,[4] Daan P. J. Swart,[4]
Andreas Richter,[5] Folkard Wittrock,[5] Anja Schoenhardt,[5] Thomas Wagner,[6]
Ossama W. Ibrahim,[7] Michel van Roozendael,[8] Gaia Pinardi,[8] James F. Gleason,[9]
J. Pepijn Veefkind,[1] and Pieternel Levelt[1]

[1]   We present a sensitivity analysis of the tropospheric NO$_2$ retrieval from the Ozone Monitoring Instrument (OMI) using measurements from the Dutch Aerosol and Nitrogen Dioxide Experiments for Validation of OMI and SCIAMACHY (DANDELIONS) and Intercontinental Chemical Transport Experiment-B (INTEX-B) campaigns held in 2006. These unique campaigns covered a wide range of pollution conditions and provided detailed information on the vertical distribution of NO$_2$. During the DANDELIONS campaign, tropospheric NO$_2$ profiles were measured with a lidar in a highly polluted region of the Netherlands. During the INTEX-B campaign, NO$_2$ profiles were measured using laser-induced fluorescence onboard an aircraft in a range of meteorological and polluted conditions over the Gulf of Mexico and the east Pacific. We present a comparison of measured profiles with a priori profiles used in the OMI tropospheric NO$_2$ retrieval algorithm. We examine how improvements in surface albedo estimates improve the OMI NO$_2$ retrieval. From these comparisons we find that the absolute average change in tropospheric columns retrieved with measured profiles and improved surface albedos is 23% with a standard deviation of 27% and no trend in the improved being larger or smaller than the original. We show that these changes occur in case studies related to pollution in the southeastern United States and pollution outflow in the Gulf of Mexico. We also examine the effects of using improved Mexico City terrain heights on the OMI NO$_2$ product.

Citation: Hains, J. C., et al. (2010), Testing and improving OMI DOMINO tropospheric NO$_2$ using observations from the DANDELIONS and INTEX-B validation campaigns, *J. Geophys. Res.*, *115*, D05301, doi:10.1029/2009JD012399.

1.   Introduction

[2]   Atmospheric nitrogen oxides (NO$_x$ = NO + NO$_2$) are precursors of tropospheric ozone, nitrate aerosol, and the hydroxyl radical (OH) which is the main atmospheric oxidant. These species affect air quality, visibility and human health. Bottom-up estimates of NO$_x$ emissions rely on extrapolation of point measurements to regional and larger scales and are thus inherently uncertain. Nitrogen dioxide (NO$_2$) absorbs light in the visible portion of the electromagnetic spectrum and can be measured as a column integral from satellite-borne solar backscatter instruments. Such measurements offer the means to derive global, top-down constraints on anthropogenic and natural emissions of NO$_x$ [*Martin et al.*, 2003; *Jaeglé et al.*, 2004]. In addition, these measurements can be used for monitoring pollution and serve as input for regional-scale forecasts. In order to use the satellite measurements reliably we need to validate the measurements and evaluate the errors associated with them. Here we use 16 lidar and 46 aircraft vertical profiles over the Netherlands and North America collected during the Dutch Aerosol and Nitrogen Dioxide Experiments for Validation of OMI and SCIAMACHY (DANDELIONS) in September 2006 [*Brinksma et al.*, 2008], and the Intercontinental Chemical Transport Experiment-B (INTEX-B) aircraft

[1]Royal Netherlands Meteorological Institute, De Bilt, Netherlands.
[2]Maryland Department of the Environment, Baltimore, Maryland, USA.
[3]Department of Chemistry, University of California, Berkeley, California, USA.
[4]RIVM, Bilthoven, Netherlands.
[5]Institute of Environmental Physics, University of Bremen, Bremen, Germany.
[6]Max-Planck Institute for Chemistry, Mainz, Germany.
[7]IUP, University of Heidelberg, Heidelberg, Germany.
[8]Belgian Institute for Space Aeronomy, Brussels, Belgium.
[9]NASA Goddard Space Flight Center, Greenbelt, Maryland, USA.

Table 1. Summary of Uncertainty Studies on Air Mass Factors due to Profile Shape

Author	Uncertainty	Retrieval	Number of Profiles	Comments	Model Used for Base Case
Heland et al. [2002]	15%	GOME NO$_2$	1	determined using one profile and surface observations.	GOMETRAN, used a fixed profile
Martin et al. [2004]	<a few percent	GOME NO$_2$	17	determined using observed profiles	GEOS-CHEM, used daily profiles
Martin et al. [2006]	9–12% (ocean-land)	SCIAMACHY NO$_2$	18	due to lightning NO$_x$, determined using actual profiles	GEOS-CHEM, used daily profiles
Bucsela et al. [2008]	10%	OMI NO$_2$	71	estimated with the averaging kernel and measured profiles.	GEOS-CHEM, used annual average profile (OMI standard product)TM4, used daily profiles (OMI DOMINO product)
Boersma et al. [2004]	<15%	GOME NO$_2$	calculated with model	theoretical study examining mixing in boundary layer and variability in NO$_2$.	TM3, used daily profiles
Schaub et al. [2006]	8%	GOME NO$_2$	157	used ground-based measurements from different altitudes in the Alps to construct a profile.	TM4, used daily profiles

campaign in spring 2006 [*Singh et al.*, 2009] to validate Ozone Monitoring Instrument (OMI) [*Levelt et al.*, 2006] retrieval sensitivity for NO$_2$. We combine the lidar observations with tropospheric NO$_2$ column densities from three MAXDOAS instruments and integrated in situ observations from a 200 m tower and compare these with OMI tropospheric NO$_2$ columns. The in situ observations were made using catalytic conversion on a heated molybdenum oxide (MoO) surface followed by ozone-induced chemiluminescence (hereafter MoO-CL). We also examine potential retrieval improvements by using the observed vertical NO$_2$ profiles in combination with improved Earth surface albedos in the OMI NO$_2$ retrieval.

[3] Recent field campaigns have been held to improve our understanding of the spatial distribution of atmospheric trace gases and to validate spaceborne observations of tropospheric composition. Previous studies used field observations from DANDELIONS, INTEX-A, INTEX-B, PAVE (Polar Aura Validation Experiment) and the North China Plain to validate OMI tropospheric NO$_2$ [*Boersma et al.*, 2008; *Brinksma et al.*, 2008; *Bucsela et al.*, 2008; *Celarier et al.*, 2008, *Irie et al.*, 2008]. These studies have found the agreement among OMI and field campaign measurements to vary with region and OMI data product used. While some of the variation may be explained by the small sample size of the measurements, all studies described above used OMI Collection 2 data that suffered from known significant across-track variability (stripes). Here we further examine results from the DANDELIONS and INTEX-B campaigns in order to test the OMI tropospheric NO$_2$ products with the most comprehensive validation set to date. We use new OMI NO$_2$ retrievals based on Collection 3 level 1B data that was released in October 2007 and which uses improved calibration of the radiance and irradiance measurements and a higher frequency of CCD background corrections than Collection 2 [*Dobber et al.*, 2008a].

[4] The dominant source of error in the tropospheric NO$_2$ retrieval over areas with enhanced NO$_2$ is the air mass factor (AMF) [*Boersma et al.*, 2004], which defines the relationship between the NO$_2$ abundance along the average photon path from the Sun through the atmosphere to the satellite (slant column) and the vertical column amount above a certain ground pixel. The AMF calculation requires external information on atmospheric scattering by air molecules,

clouds and aerosols, the shape of the NO$_2$ vertical distribution, and information on the surface albedo. The vertical distribution of NO$_2$, together with the surface albedo, represents a significant source of uncertainty in the computation of the AMF. Previous studies [*Heland et al.*, 2002; *Martin et al.*, 2004; *Boersma et al.*, 2004; *Martin et al.*, 2006; *Schaub et al.*, 2006; *Bucsela et al.*, 2008] estimate the uncertainty in the AMF due to a priori profile to be between 5% and 15% (Table 1). However, these studies were based on small samples and covered limited regions and time periods. For studies using aircraft data it was furthermore necessary to extrapolate boundary layer observations down to the surface, resulting in additional uncertainties in the profile shape [*Boersma et al.*, 2008; *Bucsela et al.*, 2008]. In this paper we use vertical profiles observed from aircraft, but also from lidar measurements, which do not require extrapolation in the boundary layer. Satellite and field observations represent the state of the atmosphere on different spatial and temporal scales. Satellite observations are a snapshot of the atmosphere over a satellite ground pixel. Ground-based observations represent different spatial scales depending on viewing direction, wind speed and integration time. In situ observations from aircraft depend on flight pattern. These limitations must be considered when comparing satellite and field campaign results.

[5] The Dutch OMI NO$_2$ product (DOMINO) [*Boersma et al.*, 2007] uses a priori NO$_2$ profiles simulated at a spatial resolution of 3° longitude by 2° latitude by TM4, a global chemistry transport model (CTM). We use the lidar and aircraft vertical profiles to evaluate the TM4 capability to appropriately simulate the a priori NO$_2$ profile shapes at the spatial scales of the OMI satellite footprints. We compare the original DOMINO tropospheric NO$_2$ and improved DOMINO tropospheric NO$_2$, recalculated using NO$_2$ profiles from field campaigns instead of simulated by TM4, to determine the sensitivity of the retrieval to the a priori profile shape.

[6] The DOMINO retrieval algorithm uses estimates of surface albedo derived from a combination of the TOMS and GOME surface reflectivity data sets [*Boersma et al.*, 2004]. These estimates are limited by the spatial resolution of the GOME climatology (1° latitude × 1.25 ° longitude) and by cloud residual features. *Kleipool et al.* [2008] recently developed a surface albedo climatology using 3 years of OMI

data with improved spatial (0.5° latitude × 0.5° longitude) resolution. Cloud contamination is a significant source of error for the calculation of surface reflection and the retrieval of trace gases. The higher spatial resolution of the OMI reflectance data set reduces cloud contamination of ground pixels as compared to TOMS/GOME. Another advantage of the *Kleipool et al.* [2008] climatology is that it represents the surface reflectance at approximately 1340 local time, consistent with all OMI observations. It includes all wavelengths specific to OMI retrievals and this reduces errors that may arise from the interpolation that is required when using the TOMS/GOME data set. Using the OMI albedo climatology for OMI NO$_2$ retrievals also reduces errors arising from unaddressed instrumental effects and long-term trends associated with TOMS/GOME but not with OMI. Using the OMI albedo climatology instead of the TOMS/GOME climatology ensures that the optimal Lambertian Equivalent Reflectivity is derived under the same illumination conditions (solar zenith angle) so that Bidirectional Reflectance Distribution Function (BRDF) effects are minimized. Theoretical studies indicate that uncertainties in the surface albedo lead to errors of 15–28% for retrievals in polluted conditions [*Martin et al.*, 2002; *Boersma et al.*, 2004].

[7] We compare field observations with four retrievals of DOMINO tropospheric NO$_2$: (1) original retrievals (Collection 3, v1.02), (2) improved retrievals accounting for observed NO$_2$ profiles only, (3) improved retrievals implementing *Kleipool et al.* [2008] surface albedos maps only and (4) improved retrievals implementing *Kleipool et al.* [2008] surface albedos maps and observed NO$_2$ profiles. We test this approach for different regions sampled during the campaigns and for special cases related to pollution in the Netherlands and the southeastern United States, transport of pollution into the Gulf of Mexico and for strongly varying terrain heights around Mexico City.

2. Data

2.1. OMI

[8] OMI is the Dutch-Finnish Ozone Monitoring Instrument on NASA's EOS Aura satellite. Aura was launched on 15 July 2004 with a Sun-synchronous polar orbit that crosses the equator at approximately 1330 local time [*Levelt et al.*, 2006]. OMI is a nadir spectrograph viewing direct and atmospheric backscattered sunlight in the UV-VIS range of 270–500 nm. The Earth shine spectrum (radiance) and direct Sun spectrum (irradiance) is collected with a CCD detector with specifications such that the ground pixel size is 13–26 km along track and 24–128 km across track depending on viewing zenith angle. Collection 3 uses an improved solar irradiance reference spectrum [*Dobber et al.*, 2008b] with improved radiometric calibration accuracy. The irradiance reference spectrum is used to optimize the OMI absolute radiometric radiance and irradiance calibration. The OMI Sun irradiance viewing angle dependence was improved. Collection 2 calibration parameters for irradiance goniometry were based on prelaunch measurements and suffered from limited angular sampling and poor signal to noise. In Collection 3 these calibration parameters are improved using in-flight irradiance measurements. Collection 3 uses an improved background correction scheme based on daily updates of the background measurements, which re-

moves most inaccuracies originating from proton radiation damage to the CCD detectors [*Dobber et al.*, 2008a].

2.2. OMI DOMINO Algorithm

[9] In this paper we present results from the OMI DOMINO Collection 3 version 1.0.2 available from http://www.temis.nl. OMI tropospheric NO$_2$ columns are retrieved by a three-step method: (1) performing a Differential Optical Absorption Spectroscopy (DOAS) fit at 405–465 nm to obtain an NO$_2$ slant column, (2) estimating the stratospheric contribution by data assimilation of slant columns in the TM4 CTM, and (3) calculating a tropospheric AMF. Slant columns are derived by a fit of OMI reflectance spectra in the 405–465 nm window [*Boersma et al.*, 2007]. The DOAS fit with OMI Collection 3 data includes reference spectra for NO$_2$, ozone, H$_2$O and the Ring effect. For the reference solar irradiance spectrum a fixed spectrum based on all OMI solar calibration measurements of 2005 is used. Because the slant columns are based on OMI Collection 3 data, the a posteriori stripe correction [*Boersma et al.*, 2007] used in earlier versions before version 1.0.0 has been switched off and this leaves some residual stripes. Stratospheric NO$_2$ is obtained by assimilating NO$_2$ slant columns with TM4 which is driven by ECMWF (European Centre for Medium-Range Weather Forecasts) meteorology. Tropospheric slant columns are calculated by subtracting the stratospheric slant column from the total slant column and are subsequently converted to vertical columns by applying the tropospheric AMF. The temperature dependence of the NO$_2$ cross section is accounted for using ECMWF temperature profiles for every OMI viewing scene as described by *Boersma et al.* [2004].

[10] The OMI sensitivity to NO$_2$ in the troposphere depends on surface albedo, clouds, aerosols and the vertical distribution of NO$_2$. This sensitivity is expressed as the AMF, the ratio of the slant column to the vertical column and is calculated with a radiative transfer model that includes estimates of surface albedo [*Koelemeijer et al.*, 2003], cloud properties [*Acarreta et al.*, 2004] and the NO$_2$ profile shape. The surface pressure and NO$_2$ profiles are obtained from TM4 on a 3° by 2° (longitude by latitude) grid scale. The model is driven by ECMWF meteorological fields, updated every 3 h in the boundary layer, at 1° by 1° resolution, aggregated to 3° by 2° resolution. When NO$_2$ is close to the surface the sensitivity of OMI is weak and the AMF is small. When NO$_2$ is higher in the atmosphere or over bright surfaces the AMF is larger. In this paper we calculate the sensitivity of the OMI tropospheric NO$_2$ product to the NO$_2$ profile shapes in the AMF for regions sampled during the INTEX-B and DANDELIONS field campaigns during spring and fall 2006. The dependence of satellite NO$_2$ on profile shape is also influenced by the surface albedo and by clouds. When the surface albedo is low, as over vegetative surfaces, there is a larger impact of the profile estimates on the AMF than when the surface albedo is higher, as over snow covered surfaces. Cases with low clouds also require accurate knowledge of the vertical distribution of NO$_2$ because the AMF is more sensitive to NO$_2$ profile shape under these conditions [*Boersma et al.*, 2004; *Schaub et al.*, 2006]. The calculation of the AMF uses the effective cloud fraction and cloud pressure of the OMI cloud product (OMCLDO2) derived from the O$_2$-O$_2$

absorption feature around 470 nm [*Acarreta et al.*, 2004; *Sneep et al.*, 2008]. In the cloud model used by the OMCLDO2 algorithm, clouds are represented as opaque Lambertian surfaces of albedo 0.8. This treatment of clouds in the cloud model is consistent with the representation of clouds in the AMF calculations.

[11] *Boersma et al.* [2007] estimated an error budget for the OMI DOMINO product. They assign a 0.7×10^{15} molecules cm^{-2} uncertainty to the slant column, a 0.15×10^{15} molecules cm^{-2} uncertainty to the stratospheric slant column and a 10–40% uncertainty to the tropospheric AMF. The uncertainty in the AMF is derived from estimates of a 15% uncertainty from surface albedo, 30% uncertainty from cloud fraction, 15% uncertainty from cloud pressure and 9% uncertainty from the profile shape. These estimates are for polluted conditions like those measured during the DANDELIONS and INTEX-B campaigns.

2.3. OMI Standard Product Algorithm

[12] The OMI standard product algorithm involves three steps, (1) obtaining a slant column identical to the OMI DOMINO product, (2) estimating the stratospheric contribution, and (3) calculating a tropospheric AMF. Estimating the stratospheric column involves converting the slant columns into initial vertical columns with an AMF accounting for an a priori stratospheric NO$_2$ profile shape. Areas of large tropospheric NO$_2$, greater than 0.5×10^{15} molecules cm^{-2}, are masked. A stratospheric NO$_2$ field is then created by smoothing the remaining initial vertical columns with a wave-2 analysis. Note that the standard product estimates the stratospheric NO$_2$ differently than the DOMINO product and these differences lead to differences in the tropospheric NO$_2$ products. *Lamsal et al.* [2010] performed a detailed analysis comparing the standard product and the DOMINO product. They found that the DOMINO product typically retrieves larger ($1–3 \times 10^{15}$ molecules cm^{-2}) stratospheric NO$_2$ than DOMINO. *Lamsal et al.* [2010] also found seasonal differences in the AMFs retrieved by the two products that resulted in seasonally different tropospheric NO$_2$ (for North America the average DOMINO tropospheric NO$_2$ was 42% larger than the standard product in winter and 22% smaller than the standard product in summer).

[13] For the standard product the stratospheric NO$_2$ field is subtracted from the initial vertical column. For areas with positive differences, a corrected tropospheric vertical column density is calculated by multiplying the initial vertical column density by the ratio of the stratospheric to tropospheric AMFs. This corrected vertical column density is the "polluted" NO$_2$ column assumed to be in the lower to middle troposphere. The tropospheric AMF is calculated using NO$_2$ profiles from the annual mean GEOS-Chem model, surface albedos from *Koelemeijer et al.* [2003] and cloud parameters from *Acarreta et al.* [2004]. The standard product and DOMINO product use the same cloud information described in section 2.2. The temperature dependence of the NO$_2$ cross section is accounted for using monthly mean NCEP temperature profiles [*Bucsela et al.*, 2006].

2.4. DANDELIONS: Campaign Overview

[14] The Dutch Aerosol and Nitrogen Dioxide Experiments for Validation of OMI and SCIAMACHY (DANDELIONS) campaigns were carried out in part to validate satellite NO$_2$ from OMI [*Brinksma et al.*, 2008]. There were two DANDELIONS campaigns held at Cabauw, the Netherlands (51.97°N, 4.93°E), one in 2005 and one in 2006, and results from the 2006 campaign are presented here. Cabauw is a suburban site and was selected with the hope that measurements made there might be representative of a larger region. Figure 1 shows the campaign location on a monthly average OMI tropospheric NO$_2$ map, illustrating the high levels of air pollution at Cabauw. The DANDELIONS campaign included ground-based measurements of NO$_2$ columns from three different Multi Axis Differential Optical Absorption Spectrometers (MAXDOAS) operated by different research groups [*Wagner et al.*, 2004; *Wittrock et al.*, 2004; *Pinardi et al.*, 2008]. During the campaign a lidar collected lower tropospheric NO$_2$ profiles [*Volten et al.*, 2009] and these profiles have been compared to independent measurements as described by *Brinksma et al.* [2008]. *Brinksma et al.* [2008] presented first results from the lidar and compared lidar and MoO-CL observations and lidar and MAXDOAS columns providing some confidence that overall lidar profiles are reliable. A second lidar continuously monitoring aerosols between the surface and 14 km was employed during the campaign providing planetary boundary layer height estimates [*Apituley et al.*, 2000; *Schaap et al.*, 2009]. The DANDELIONS campaign was carried out in September 2006. During the campaign there were 9 days with minimal cloud cover, a condition necessary for satellite validation of tropospheric trace gas estimates, and these occurred on 8–13 September and 20–22 September. Table 2 presents an overview of the instruments used to measure NO$_2$ profiles and column contents during the DANDELIONS and INTEX-B campaigns. The lidar and MoO-CL instruments provide vertical distributions of NO$_2$ and the MAXDOAS instruments provide tropospheric NO$_2$ columns. Details of the ground-based instruments are described below. The MAXDOAS, lidar and MoO-CL observations all have their own characteristic strengths and weaknesses. None of these techniques represent a standard, yet they represent three independent ways to observe tropospheric NO$_2$. Because tropospheric NO$_2$ profile and column observations have only limited availability we use them as a starting point for the testing and improvement of satellite algorithms.

2.4.1. MAXDOAS Instruments

[15] During the DANDELIONS campaign the Belgian Institute for Space Aeronomy (BIRA) and Bremen University operated MAXDOAS instruments to retrieve NO$_2$ columns. The University of Heidelberg operated a MAXDOAS instrument that simultaneously viewed three azimuth directions. Detailed descriptions of the instruments are given by *Wagner et al.* [2004], *Wittrock et al.* [2004], *Brinksma et al.* [2008] and *Pinardi et al.* [2008]. MAXDOAS instruments used in the DANDELIONS campaign made consecutive measurements of scattered solar radiation, with a spectral range of 407–497 nm, at increasing telescope elevation angles from 15°, 30° and 90°. Total slant column densities are determined with DOAS, but the different instruments use different spectral windows. The MAXDOAS slant column is converted to a tropospheric vertical column using a geometric AMF as described by *Brinksma et al.* [2008]. The MAXDOAS instruments viewed different azimuth directions at Cabauw, with the BIRA instruments pointing south, the
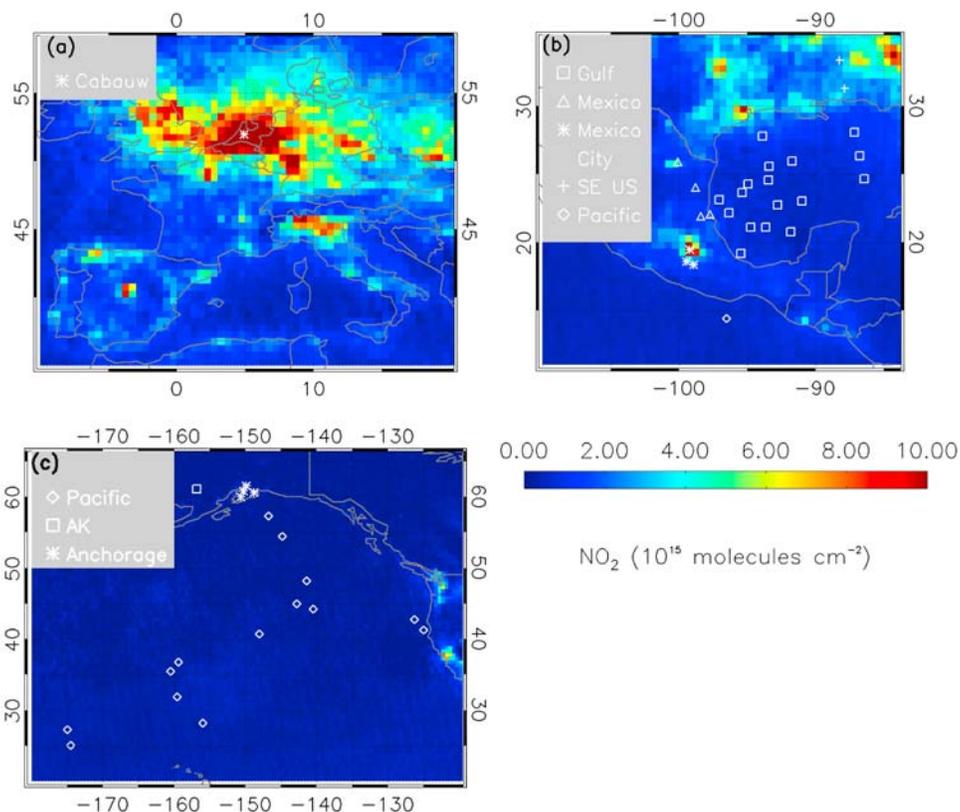
Figure 1. Regional maps of OMI DOMINO tropospheric monthly average NO_2 over (a) Europe for September 2006, (b) the Gulf of Mexico for March 2006, and (c) the Pacific for April 2006. Symbols denote the different locations of INTEX-B profiles and Cabauw, Netherlands. AK is Alaska.

Bremen instrument pointing west-southwest, and the Heidelberg instrument pointing west-northwest, south-southwest and east-southeast. We estimate the uncertainty associated with the MAXDOAS measurements to include fitting errors (~5%), systematic errors in temperature and cross sections (~10%), AMF uncertainties (~20%) and horizontal variability in combination with time differences between the off axis and zenith measurement (~10%) yielding a 25% approximate error. The uncertainty in the AMF may be larger (~30%) under conditions with elevated aerosols because multiple scattering effects are not accounted for with the simplified geometric AMF.

2.4.2. RIVM MoO-Conversion-Chemiluminescence Instrument for NO_2

[16] Concentrations of atmospheric NO_2 were measured with standard in situ MoO-CL instruments using molybdenum oxide converters. In this instrument NO_2 is catalytically converted to NO on a 315°C heated molybdenum surface and then measured as NO by chemiluminescence after reaction with ozone. The molybdenum converter also partly converts other oxidized nitrogen compounds such as nitric acid (HNO_3), alkyl nitrates, and peroxyacetyl nitrate (PAN) to NO [*Steinbacher et al.*, 2007; *Dunlea et al.*, 2007, and references therein]. This conversion causes NO_2

Table 2. Summary of Instruments Used to Measure NO_2 Profiles and Columns During the INTEX-B and DANDELIONS Campaigns

Technique	Vertical Domain	Region	Validated Technique
MAX-DOAS	tropospheric column	Netherlands	presented by *Brinksma et al.* [2008] and *Celarier et al.* [2008]
MoO-CL	boundary layer column from 0 and 0.2 km observations	Netherlands	possible 30% high bias to interfering species[a]
lidar	vertical distributions[b] 0–5 km	Netherlands	presented by *Volten et al.* [2009] and *Brinksma et al.* [2008]
LIF/DC-8	vertical distributions[b] 0.15 km over ocean (0.3 km over land): 11 km	southeastern U.S., Gulf of Mexico, Mexico City, Pacific	presented by *Boersma et al.* [2008] and *Bucsela et al.* [2008]

[a]Thirty percent bias is from interference of oxidated nitrogen compounds whose presence depends on air mass history [*Steinbacher et al.*, 2007], though this was determined for a different region. Using the CHIMERE model, we estimate that the bias is 10–20%.
[b]Lidar does not sample the full free troposphere and the LIF onboard the aircraft misses the lowest portion of the boundary layer.

concentrations to be overestimated, especially in photochemically aged air masses. *Steinbacher et al.* [2007] have shown overestimations up to 30% at rural locations downwind of pollution sources in Switzerland. For urban air in Mexico City, *Dunlea et al.* [2007] found no significant bias in the morning but increasing bias in the afternoon, presumably reflecting the diurnal formation of NO$_x$ oxidation products. Not all chemiluminescence methods suffer from these interferences; *Fehsenfeld et al.* [1990] describe a photolytic chemiluminescence instrument that compared well with a tunable diode laser absorption spectrometer which does not suffer from the interferences.

[17] To account for the bias in NO$_2$ observations from the MoO-CL monitors we have applied the correction factor, cf, described by *Lamsal et al.* [2008],

$$cf = \frac{NO_2}{NO_2 + 0.95 \times PAN + 0.32 \times HNO_3}. \quad (1)$$

[18] Here NO$_2$, PAN (peroxyacetlynitrate) and HNO$_3$ (nitric acid) are retrieved from the regional CHIMERE model [*Blond et al.*, 2007] and the 0.95 and 0.35 refer to conversion efficiencies of those species on the molybdenum oxide converter. The cf calculated at Cabauw for September is 0.885 ($\pm$0.1). We apply this correction factor to all MoO-CL observations. These corrections showed good agreement with corrections inferred from simultaneous measurements from MoO-CL and photolytic chemiluminescence instruments in Taenikon, Switzerland [*Steinbacher et al.*, 2007; *Boersma et al.*, 2009].

[19] During the DANDELIONS campaign one MoO-CL was placed on the ground and another was placed on top of the 200 m tower at Cabauw. In order to compare these measurements with OMI tropospheric NO$_2$ columns, the MoO-CL NO$_2$ density was extrapolated from 200 m to the top of the boundary layer (measured with the aerosol lidar), linearly interpolated between the surface and 200 m and then integrated to obtain a planetary boundary column content. Note that the column densities calculated with the MoO-CL observations do not account for free tropospheric NO$_2$. The uncertainty associated with the MoO-CL monitor integrated columns is dominated by interference from NO$_y$ species and extrapolation of the observations to the planetary boundary layer. The uncertainty associated with the boundary layer top should be small because this was measured with the RIVM boundary layer lidar described in section 2.4.3. We find that the observations made at 200 m were 10–35% larger than those at the surface and we use this to estimate uncertainties associated with extrapolation within the boundary layer to be around 30%. Because the clear-sky days in September 2006 had little influence of nearby lightning, and because of the high concentrations of NO$_2$ in the Cabauw boundary layer (on average 5 ppb) we believe that the possible bias introduced by not accounting for free-tropospheric NO$_2$ [e.g., *Hudman et al.*, 2007; *Napelenok et al.*, 2008] is relatively small. This will be discussed in more detail in section 2.4.3.

2.4.3. RIVM NO$_2$ and Aerosol Lidars

[20] The RIVM NO$_2$ lidar uses the Differential Absorption Lidar (DIAL) technique to observe vertical profiles of NO$_2$ [*Brinksma et al.*, 2008; *Volten et al.*, 2009]. The emitting unit uses a dye laser to send out a narrow pulsed beam of light at different elevation angles. The laser is first tuned to 449.10 nm, where NO$_2$ absorption is strong, then detuned to 448.31 nm, where absorption is weak. The backscattered light is collected as a function of time and used to calculate a vertical NO$_2$ profile. The typical lidar configuration samples the atmosphere with the telescope aimed to the zenith. Because of incomplete overlap between the backscattered signal and the field of view of the telescope, the telescope is blind to atmospheric absorbers in the first 300 m. At Cabauw, the first 300 m of the atmosphere contain large quantities of NO$_2$ and in order to sample this layer the RIVM group developed a different lidar configuration. During DANDELIONS the lidar was aimed at 7 different elevation angles to obtain a profile of NO$_2$ at altitude ranges with centers at ~20, 40, 75, 150, 300, 570 and 1400 m above ground. Lidar profiles have a spatial representativity of 2 km in viewing direction and approximately 12 km in the direction of the wind [*Volten et al.*, 2009]. The 12 km depends on the wind speed, because during typical lidar integration times (40 min), significant averaging over air masses passing the field of view of the lidar takes place. The precision related to instrumental noise is 0.2–0.4 μg m^{-3} or around 10% of the concentrations observed at Cabauw. Systematic errors associated with uncertainty in the cross section measurements are approximately 10%.

[21] *Volten et al.* [2009] compared lidar observations with the MoO-CL observations made at the corresponding altitudes and times. They found good agreement among the two instruments in the morning when interfering species (NO$_y$) are expected to have a minimal presence. In situations when the lidar and MoO-CL agreed the CHIMERE regional model indicated that few interfering compounds were present. For comparisons between MoO-CL and lidar where agreement was not good, CHIMERE output showed higher concentrations of interfering compounds.

[22] RIVM also collected aerosol backscatter measurements with an aerosol lidar. The aerosol lidar uses a Nd-YAG laser to send pulses of 1064 nm light into the atmosphere. The intensity of the backscatter signal and the time the signal is received are used to determine the relative amount of aerosol and the aerosol altitude. This instrument provides information on the boundary layer height, overhead clouds, and the vertical aerosol distribution with high temporal resolution (5 min). The height of the planetary boundary layer is determined from these measurements with a typical precision of 50 m, and used in the integration of the NO$_2$ lidar and MoO-CL measurements. NO$_2$ lidar measurements were extrapolated to the top of the planetary boundary layer and to the surface for integration. We do not include assumptions about upper level free tropospheric NO$_2$ in the integrated lidar profile and this could add a bias to these observations. An upper limit for this bias would be 1.0 $\times$ 10^{15} molecules cm^{-2} based on aircraft observations over the summertime southeastern United States where lightning activity is at its peak [*Napelenok et al.*, 2008], but for the DANDELIONS cases the bias is likely smaller because the clear-sky days during DANDELIONS had little influence of nearby lightning. TM4 free tropospheric NO$_2$ ranged from 0.1 to 0.7 $\times$ 10^{15} molecules cm^{-2} for corresponding lidar observations and on average added 0.4 $\times$ 10^{15} molecules cm^{-2} to the lidar observations.

Table 3. Summary of Analysis Methods and Results Comparing LIF/DC-8 NO$_2$ With OMI Tropospheric NO$_2$[a]

Author	Method for Extrapolating LIF Profile	OMI Selection	Slope (y axis = OMI SP)	LIF-OMI SP Correlation Coefficient (r)	Slope (y axis = OMI DOMINO)	LIF-OMI DOMINO Correlation Coefficient (r)	Number of Profiles Compared
This work	Values extrapolated to aircraft measured surface. For one case over Mexico LIF values were extrapolated to OMI high-resolution surface	OMI Collection 3. Cloud radiance fraction <0.5. Pixels overlapping any portion of aircraft profile from 0 to 3 km.	0.59 ± (0.10)	0.78	0.87 ± (0.29)	0.74	46
Boersma et al. [2008]	Values extrapolated 300 m below lowest observation over land and 150 m below lowest observation over oceans.	OMI Collection 2. Cloud radiance fraction <0.5. Pixels with center coordinates <0.1° from lower-level aircraft observations.	NA	NA	1.40 ± (0.21) 0.99 ± (0.17)	0.79 0.67	21 12
Bucsela et al. [2008]	Values extrapolated using LIF measurements and model profile shapes. Surface pressures are NCEP monthly means.	OMI Collection 2. Cloud fraction <0.3. Pixels with center coordinates <0.2° from lower-level aircraft observations.	0.86 ± (0.20)	0.83	1.68 ± (0.60)	0.83	71 (58)[b]

[a]The present work and *Boersma et al.* [2008] both use an unweighted RMA fit, and *Bucsela et al.* [2008] weight the data with *x, y* error estimates.
[b]*Bucsela et al.* [2008] compared 71 LIF/DC-8 profiles with OMI SP data and 58 LIF/DC-8 profiles with OMI DOMINO data.

2.5. Aircraft Profiles Made During INTEX-B

[23] During INTEX-B the University of California at Berkley Laser-Induced Fluorescence instrument onboard the NASA DC-8 aircraft (LIF/DC-8) measured in situ NO$_2$. The aircraft made flights over the Gulf of Mexico, Mexico City, the southeastern United States, and the Pacific. The locations of profiles made during flights are shown in Figure 1 with monthly average OMI DOMINO tropospheric NO$_2$ maps for March and April 2006. The LIF/DC-8 instrument is described in detail by *Thornton et al.* [2000] and analysis of the data has been performed by *Bucsela et al.* [2008] and *Boersma et al.* [2008]. In brief, the LIF/DC-8 instrument samples air continuously and a tunable dye laser set at 585 nm is used to excite NO$_2$ in the sampled air stream. The laser is alternately tuned between peak and weak absorption of NO$_2$. The ratio of NO$_2$ fluorescence at the two frequencies is proportional to the NO$_2$ mixing ratio. The precision at a 1 Hz sampling rate ranges from ±23 ppt at 1000 hPa to ±46 ppt at 200 hPa (S/N = 2). The detection limits are estimated to be 3 ppt at the ground and 6 ppt at 12 km [*Bucsela et al.*, 2008].

[24] We convert airborne LIF/DC-8 measurements of NO$_2$ mixing ratios into column contents and we estimate the missing portion of the profile below 300m and up to the tropopause, assumed to be 12 km. We used DC-8 airborne RADAR observations of altitude above ground level to extrapolate to the surface the median of the 10 lowest altitude mixing ratio measurements. For cases near Mexico City where there are large variations in terrain height we extrapolate to the OMI high-resolution terrain heights. *Bucsela et al.* [2008] made extrapolations to ground by combining medians of low-altitude mixing ratios with modeled annual mean profile shapes from GEOS-Chem, scaled to the LIF measurements. A noteworthy difference is that the *Bucsela et al.* [2008] extrapolation relied on surface pressure estimates from NCEP monthly means that were sometimes smaller than the values of the bottom pressure of the aircraft profile. NO$_2$ columns near Mexico City with the largest

column contents were influenced by these surface pressure estimates. However, in spite of such pressure discrepancies, the average of their extrapolations to the ground was slightly larger than in the present study. Our extrapolation approach is also different from *Boersma et al.* [2008] because they extrapolated NO$_2$ subcolumns to 150 m below the lowest aircraft altitude over the ocean and 300 m over land, based on aircraft flight restrictions, instead of actually observed RADAR altitudes. Table 3 summarizes the methods of integration and results from the present study, *Boersma et al.* [2008] and *Bucsela et al.* [2008]. Some of the DC-8 spirals sample across the edges of significant plumes. For example, a profile may begin at the north end of an urban plume and end at a southern end near a marine layer. We have examined the 10 points used for extrapolation in each profile and found the variations among the points to be small for all cases except two flights near Mexico City. For these two cases the aircraft performed a transect through the boundary layer and we averaged all mixing ratio observations made in this transect and extrapolate this average mixing ratio to the surface. Extrapolating to the surface accounts for an average of 16% of the column content though the extrapolation can account for as much as 70% of the column for some individual columns. For columns larger than 2×10^{15} molecules cm^{-2} the extrapolation to the surface accounts for an average of 20% of the column. The top of the aircraft profiles varied from 2 to 12 km. There is much less variation in free tropospheric NO$_2$ than in boundary layer NO$_2$. To make aircraft profiles commensurate with one another, we extrapolated the median NO$_2$ mixing ratio from the 10 highest altitude observations up to 12 km, which we assume to be the top of the troposphere. If the median mixing ratio to be extrapolated was less than the LIF/DC-8 detection limit (3 ppt) we used half of the detection limit. Extrapolating to 12 km accounts for an average of 25% of the column, though the extrapolation can account for as much as 83% for an individual column. Our approach differs from that of *Bucsela et al.* [2008], who based their extrapolations to the tropopause

on daily means of LIF measurements made at nearby locations, where available, and on scaled model profiles elsewhere. Their upper tropospheric extrapolations were smaller, on average, than the ones computed in our study. We converted the NO$_2$ mixing ratios (in ppb) to molecules cm^{-3} using observed pressure and temperature data and then integrated the NO$_2$ profile from the surface to 12 km. Because NO$_2$ is highly variable in the lower planetary boundary layer we limit the analysis to flights with profiles that sampled at least as low as 500 m above the surface.

[25] During the INTEX-B campaign the aircraft profile often covered an area larger than a single OMI ground pixel. For these comparisons OMI ground pixels were chosen if they overlapped the portion of the aircraft profiles made between the surface and 3 km. The terrain around Mexico City is highly variable and for these flights we chose OMI pixels that overlapped portions of the flights made in the boundary layer only. These selection criteria are different from *Bucsela et al.* [2008] and *Boersma et al.* [2008] because they used OMI pixels with center coordinates within 0.2° and 0.1° of lower-level aircraft observations. For this paper we only used OMI observations made within ±3 h of aircraft measurements. Because the OMI NO$_2$ algorithm is highly sensitive to clouds we only use OMI data with cloud radiance fractions smaller than 0.5. *Bucsela et al.* [2008] used a less strict geometric cloud fraction filter of 0.3 corresponding to cloud radiance fractions of 0.6–0.7 or higher. We found 46 INTEX-B profiles to compare with OMI ground pixels given the above restrictions and this sample size is smaller than that of *Bucsela et al.* [2008] and larger than that of *Boersma et al.* [2008].

[26] To calculate the uncertainty associated with the LIF/DC-8 NO$_2$ columns, we must account for the accuracy of the instrument which *Day et al.* [2002] determined to be 5% as well as the uncertainty associated with extrapolating the NO$_2$ to the surface and to 12 km. *Boersma et al.* [2008] and *Bucsela et al.* [2008] assign respective uncertainties of 75% and 80% to the extrapolated portions, based on GEOS-Chem modeled variability. We include similar estimates in our uncertainty estimation. We calculate the total uncertainty ε in the LIF/DC-8 columns with the following:

$$\varepsilon = 0.05 \times N_m + 0.75 \times N_{ext}. \qquad (2)$$

[27] Here N$_m$ is the portion of the column that is directly measured and N$_{ext}$ is the portion of the column that is extrapolated, either to the surface or to 12 km. The uncertainty associated with the columns ranges from 7 to 66% with an average of 33%. This error analysis is included to provide the reader with an estimate of the quality of the data. However, we have not included this error in the regression analysis presented below.

3. Comparisons With OMI

3.1. Ground-Based Comparisons With OMI During DANDELIONS

[28] Figures 2a and 2b show comparisons of all of the tropospheric NO$_2$ column data sets derived from ground-based observations with OMI DOMINO (Figure 2a) and with OMI standard product tropospheric NO$_2$ (Figure 2b).

Comparisons of OMI DOMINO with ground-based observations have slopes ranging from 0.56 (MAXDOAS) to 1.8 (lidar) with correlation coefficients ranging from 0.43 to 0.80. These slopes were calculated using the reduced major axis regression (RMA) [*Clarke*, 1980] that minimizes the joint deviation of both variables from the regression model without attributing weights to the data. We employ the RMA regression because no clear distinction can be drawn between OMI and DANDELIONS tropospheric NO$_2$ columns in terms of their dependency relations; both have considerable uncertainty estimates, see error bars in Figures 2c and 2d, and there is considerable uncertainty in these estimates. The MoO-CL NO$_2$ is sometimes larger than OMI and the other instruments. This is presumably due, in part, to the known interference from other nitrogen oxide species in the nonspecific surface conversion on heated MoO converters. The lidar typically observes less NO$_2$ than OMI and the other instruments. The ground-based instruments at Cabauw observed in different azimuthal directions and other studies have shown large variations in NO$_2$ observed from different directions [*Brinksma et al.*, 2008; *Celarier et al.*, 2008; *Volten et al.*, 2009].

[29] We average these observations per day, to increase the representativeness of these observations toward the OMI ground pixel coverage (Figures 2c and 2d). By averaging over the various measurement techniques, we also average any systematic biases per system and this must be considered when examining the significance of the resulting slopes and correlation coefficients. There are significant uncertainties associated with the slopes presented here and they are estimated with 2 times the standard deviation (95% confidence levels assuming normal distributions).

[30] Figures 2c and 2d shows comparisons of the daily average of all ground-based observations with OMI tropospheric NO$_2$ and shows correlations of 0.77 (n = 16) and 0.81 (n = 16) for OMI DOMINO and standard product NO$_2$. A single OMI ground pixel with center coordinates closest to Cabauw was chosen to compare with daily ground-based observations and only OMI ground pixels with overpass times within 1 h of ground-based measurements were used. Figures 2c and 2d suggest that for this small data set the size of the OMI ground pixel does not appear to affect the agreement among OMI NO$_2$ and ground-based observations. The slopes for the comparison of the OMI DOMINO product and ground-based observations are close to unity, 1.07 ± 0.37 for DOMINO and 0.87 ± 0.25 for the standard product, though the sample size is small (n = 16) and the error on the slopes is 2 standard deviations. *Brinksma et al.* [2008] found correlation coefficients of 0.5–0.6 and slopes of 0.4–0.85 between OMI Collection 2 tropospheric NO$_2$ columns and MAXDOAS observations, collected in 2005 and 2006. We find no significant differences between OMI Collection 3 and Collection 2 for this location and study period. Therefore we attribute the differences in results between this and previous work to the differences in data treatment. Specifically we only examined data from 2006 and also included MoO-CL and lidar column contents in our comparisons.

[31] The error in the ground-based observations includes the following.

[32] 1. The first source of error comes from not accounting for upper tropospheric NO$_2$ in the integration of lidar and
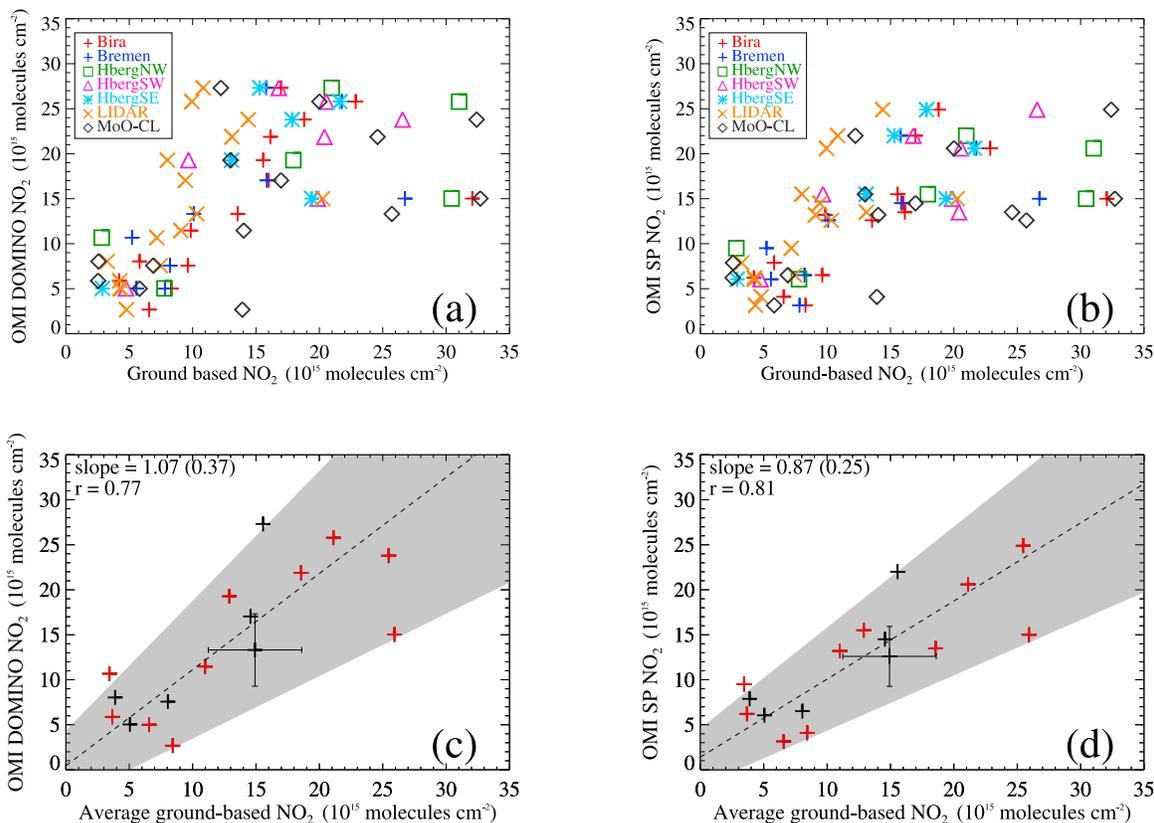
Figure 2. Comparison of all ground-based tropospheric NO$_2$ column contents made during the DANDELIONS 2006 campaign with (a) OMI DOMINO product and (b) OMI standard product. In Figures 2a and 2b the different colors denote the different instruments. The correlation coefficients for these plots range from 0.43 to 0.80. Also shown are comparisons of the daily average of all ground-based measurements with (c) OMI DOMINO product and (d) OMI standard product. In Figures 2c and 2d, red crosses denote satellite ground pixels with widths larger than 50 km, and black crosses denote satellite ground pixels with widths smaller than 50 km. We chose the 50 km width criterion because in one OMI swath 75% of OMI ground pixels have widths smaller than 50 km (corresponding to a viewing zenith angle of 44°). The error bars are shown for a single point in Figures 2c and 2d. The error bar in OMI is from the OMI retrieval precision. The error bar for the ground-based observation is the standard deviation of the mean of the observations. For Figures 2c and 2d the reduced major axis regression is shown with a dashed line, and this regression does not account for uncertainties in either x or y. The gray shading represents ±2 standard deviations of the regression. For the DANDELIONS campaign, ground-based measurements were made at a point location in Cabauw, Netherlands, and the OMI ground pixel with center coordinates closest to Cabauw was chosen for the comparison. All ground-based observations were made within 1 h of the OMI overpass and during clear-sky episodes.

MoO-CL observations. We used TM4 to estimate free tropospheric NO$_2$ and added this to the lidar and integrated MoO-CL observations. This increased the average of ground-based observations by 1–10% and improved agreement with OMI.

[33] 2. The second source of error comes from uncertainty associated with the geometric AMF used in the MAXDOAS observations.

[34] 3. The third source of error comes from uncertainty of how the MoO-CL correction factor accounts for interference in the instrument observations.

[35] These uncertainties may partly explain the scatter between ground-based observations and OMI. A constant correction factor of 0.885 cannot take into account fully the overestimation of the MoO-CL monitor observations. In

future campaigns we will therefore use in situ monitors with a photolytic converter that do not suffer from NO$_y$ interference. The spread between the other different ground-based instruments is also larger than expected. These discrepancies may result from spatial variability in the NO$_2$ field, from instrumental errors or from imperfections in the algorithms used in the analysis. It is therefore desirable that the different ground-based techniques are compared in more detail in a future campaign. We have scheduled such a campaign, CINDI, for the summer of 2009 at Cabauw. We have tested the effect of removing the MoO-CL from the average ground-based observations and found only a minor change in the slope and correlation between OMI and ground-based observations (both the slope and correlation increased by 5%).
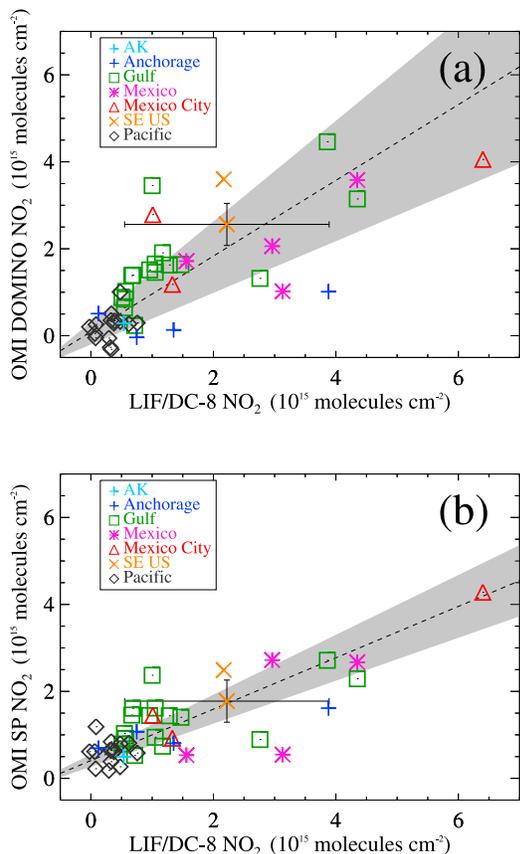
Figure 3. Comparisons of integrated LIF/DC-8 tropospheric NO₂ columns with (a) OMI DOMINO and (b) OMI standard product. The reduced major axis regression is shown with the dashed line, and this regression does not account for uncertainties in either x or y. The gray shading represents ±2 standard deviations of the regression. The correlation is larger than 0.74 for both OMI data products and the number of samples is 46. The OMI standard product NO₂ is smaller than the DOMINO product. The different locations where profiles were made are colored, and the inset denotes the color for each location. Error bars are shown for one comparison. Here the OMI error bar represents the standard deviation of the mean of OMI observations. The LIF/DC-8 error bar was calculated using equation (2).

[36] Both satellite and MAXDOAS retrievals are potentially affected by aerosols [*Martin et al.*, 2002, *Boersma et al.*, 2004, *Wagner et al.*, 2007]. Aerosol information at Cabauw is provided by the aerosol lidar and AERONET observations. We found increasing differences between OMI NO₂ and ground-based observations with increasing aerosol optical depths, but our sample was small (9 different days). On days with larger aerosol optical depths the OMI NO₂ values were typically smaller than the ground-based observations. This finding may be attributed to aerosol-induced errors in both the OMI NO₂ and in the MAXDOAS observations. This issue will be further examined at the upcoming CINDI (Cabauw Intercomparison of Nitrogen Dioxide Instruments, http://www.knmi.nl/samenw/cindi/) campaign to be held at Cabauw in summer 2009 which will increase the number of days with different aerosol loadings,

and includes a suite of instruments with very different sensitivities to aerosols.

3.2. Aircraft Profile Comparisons With OMI During INTEX-B

[37] Figure 3 shows comparisons among LIF/DC-8 integrated NO₂ and OMI DOMINO, and LIF/DC-8 and OMI standard product tropospheric NO₂. The correlation is good for both OMI products, r > 0.74. The slope for the LIF/DC-8 and OMI DOMINO NO₂ is 0.87 ± 0.29 (OMI on y axis, LIF/DC-8 on x axis) and 0.59 ± 0.10, for the LIF/DC-8 and OMI standard product NO₂. These differences in slopes are related to the different ways the two algorithms retrieve tropospheric NO₂. We performed a bootstrapping method on comparisons among OMI and LIF/DC-8 NO₂. We randomly sampled 23 of the 46 data points without replacement and calculated the correlation coefficient and RMA slope. We performed this sampling 10,000 times and the average slope for LIF/DC-8 and OMI DOMINO is 0.90 ± 0.28 with a correlation coefficient of 0.73 ± 0.18. The uncertainty here is 2 times the standard deviation of the slope and correlation coefficient. We performed the bootstrapping method on the OMI standard product and LIF/DC-8 data as well and the average slope is 0.57 ± 0.11 with a correlation coefficient of 0.74 ± 0.23. This provides a test for the robustness of the correlation coefficient and the slope. Table 1 provides a summary of results from the present study and *Boersma et al.* [2008], and *Bucsela et al.* [2008]. Taken together, these studies suggest that the NO₂ values from OMI SP are smaller than both DOMINO NO₂ and the LIF columns for the limited number of times and locations examined in these studies. Possible reasons for the different slopes presented in Figure 3 and those presented by *Bucsela et al.* [2008] and *Boersma et al.* [2008] include the extrapolation procedure, the number of profiles compared and the use of OMI Collection 2 or Collection 3. We compared OMI Collection 2 to OMI Collection 3 for 408 OMI ground pixels examined during INTEX-B and we find that OMI DOMINO Collection 2 has 10% less data than Collection 3 and OMI standard product Collection 2 has 18% less data than Collection 3. The amount of data was determined by counting the ground pixels without fill values. The smaller amount of data in Collection 2 than in Collection 3 may be related to improvements in the CCD dark current correction. We do not find any significant differences between the OMI tropospheric NO₂ values from Collection 2 and Collection 3 for either product.

[38] Our OMI ground pixel selection criteria are stricter than those used by *Bucsela et al.* [2008] and *Boersma et al.* [2008] and this partly explains the differences in linear regressions. In some cases, the stricter criteria (for pixel selection, cloud radiance fraction and time differences between OMI and aircraft observations) led to elimination of profiles used by *Bucsela et al.* [2008] and *Boersma et al.* [2008]. Overall, the most significant reasons for the smaller slopes here compared to *Bucsela et al.*'s [2008] are differences in the number of profiles used, the regression technique, and the extrapolation methods used for the upper and lower portions of the profiles. In particular, our method for extrapolating the mixing ratio to the tropopause results in generally larger tropospheric columns than obtained by *Bucsela et al.* [2008].
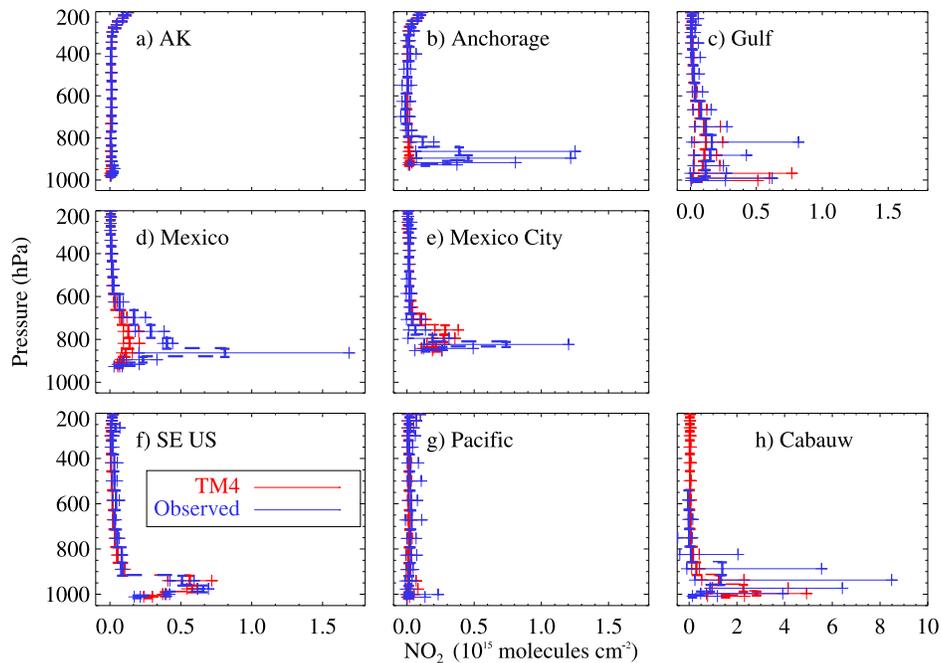
Figure 4. Average NO$_2$ profiles from TM4 shown in red and LIF/DC-8 shown in blue over regions of (a) Alaska (AK), (b) Anchorage, (c) Gulf of Mexico, (d) Mexico, (e) Mexico City, (f) southeast United States (SE U.S.), (g) Pacific, and (h) Cabauw, Netherlands. For Cabauw the average lidar partial NO$_2$ column is shown in blue. The *x* axis here shows the partial column NO$_2$ in one layer of the TM4 vertical pressure grid, and the vertical error bars represent the pressure range over which the column content extends. The choice of vertical TM4 layers is based on the hybrid sigma-pressure coordinate system employed by the ECMWF model (see *Krol et al.* [2005] for further discussion). The horizontal error bars show the minimum and maximum NO$_2$ values at the specified level. The dashed lines between pressure levels have been added as a guide to the eye.

[39] The extrapolations also complicate calculation of the LIF column errors. Since these errors as well as those associated with the OMI data are difficult to estimate accurately and can significantly affect the linear regressions [see *Bucsela et al.*, 2008] we have chosen not to use them in weighting the data for our linear regressions. Nonetheless, in spite of the uncertainties in the integration of the LIF observations, the profile shape can still be used to assess how well TM4 simulates an a priori profile for OMI retrievals.

[40] While the number of samples for the INTEX-B case is 3 times that of the DANDELIONS case it should be noted that there are only 46 observations in total. Limitations of this comparison include a smaller range of measurements where the largest NO$_2$ column observed is 9 × 10^{15} molecules cm^{-2} compared to the largest NO$_2$ observed during DANDELIONS of 27 × 10^{15} molecules cm^{-2}. In this section we have shown that OMI compares on average well with independent measurements, but there is still considerable scatter. In the following sections we will investigate whether improvements can be made in OMI satellite data by ground-based NO$_2$ profile shapes collected during both field campaigns.

4. Changes to the AMF

[41] In the next section we discuss the differences among TM4 NO$_2$ profile retrievals and those measured by the NO$_2$

lidar in the Netherlands and profiles measured with the LIF onboard the DC-8 around North America.

4.1. Comparison of TM4 and Field Campaign NO$_2$ Profiles

[42] Figure 4 shows the profile averages for TM4, LIF/DC-8 and lidar, with error bars representing the maximum and minimum, for each region analyzed in this study. In all cases, the TM4 a priori profile appears to captures the shape of the NO$_2$ profile in the boundary layer reasonably well, especially considering the time difference between TM4 (sampled at 1330 local time) and the observations can be as large as 3 h and the observed profiles are local compared to the simulated profiles that represent a 3° by 2° grid cell. There is very good agreement among the TM4 and LIF/DC-8 profiles for the Pacific, southeastern United States, the Gulf of Mexico and Alaska. For Anchorage, TM4 does not capture enhanced NO$_2$ concentrations in the boundary layer because the signature of these relatively small, isolated NO$_x$ sources is diluted over the spatial extent of a 3° × 2° grid cell. For Mexico and Mexico City, TM4 properly simulates the shapes of the NO$_2$ profile in the boundary layer but the NO$_2$ concentrations are too low. This is likely due to TM4's inability to resolve horizontal gradients within strong source regions (the problem is larger in Mexico City than over the Mexican mainland). The EDGAR 1995 emission inventory, used in the model, may underestimate Mexican NO$_x$ emissions in the year 2006 because of

known increases in NO$_x$ emissions [*van der A et al.*, 2008] in this area. For Cabauw, the simulated and observed NO$_2$ amounts agree well, but their vertical distributions within the boundary layer differ. NO$_x$ reduction strategies have been employed in the United States and the Netherlands since 1995 and this may partly explain why this older emission inventory works better for these regions. The TM4 profiles show a strong vertical gradient, whereas the observed profiles suggest that NO$_2$ is better mixed in the boundary layer over the Netherlands. We show in the following sections that the TM4 a priori profile agrees well with the LIF/DC-8 profile for conditions where the observed profile is likely representative of a regional profile (the Pacific, southeastern United States, the Gulf of Mexico and Alaska). We also show cases where the TM4 a priori profile is very different from the observed profile and we quantify how this affects the OMI NO$_2$ retrieval.

[43] For the AMF calculation for cases where the lidar (LIF/DC-8) did not observe the full free troposphere, the lidar (LIF/DC-8) partial columns were combined with TM4 NO$_2$ in the free troposphere to create a lidar TM4 (or LIF/DC-8-TM4) composite. We do not use extrapolated portions of profiles in the AMF calculation because they contain significant uncertainties and the aim of the paper is to investigate how the observed profiles affect the AMF.

4.2. How Profile Changes Affect AMF

4.2.1. Comparison of TM4 and Lidar Profiles and Resulting AMFs

[44] Figures 5a and 5c show the TM4 and lidar profiles observed during the DANDELIONS campaign for a relatively clean day on 9 September 2006 where surface NO$_2$ measured with the lidar is 3 μg m^{-3} and a polluted day on 12 September 2006 where surface NO$_2$ measured with the lidar is 20 μg m^{-3}. The boundary layer heights measured with the aerosol lidar are shown with a black line. Also shown in Figure 5 are the AMFs and OMI NO$_2$ calculated with the TM4 profile (original) and lidar profile (improved). For brevity we refer to the original DOMINO OMI tropospheric NO$_2$ as original OMI and to DOMINO OMI tropospheric NO$_2$ determined with changes to the AMF as improved OMI. For the relatively clean day, TM4 overestimates the NO$_2$ near the surface resulting in the original AMF being too small. The AMF calculated with the lidar profile (improved AMF) is larger and the improved OMI is smaller than the original OMI. In this case the improved OMI NO$_2$ column is closer to ground-based observations than the original OMI. In this case the TM4 a priori profile shape is similar to what is measured by the lidar though the concentrations are different. For this case improved OMI is 17% smaller than original OMI.

[45] Figure 5c shows the TM4 and lidar profiles for a relatively polluted day on 12 September 2006. In this case TM4 estimates that most of the NO$_2$ is lower in the atmosphere near the surface while the lidar observes NO$_2$ higher in the atmosphere near the boundary layer top. The original AMF is too small and the original OMI NO$_2$ is too large compared to ground-based observations. TM4 may not simulate boundary layer mixing properly which may partly explain the different NO$_2$ profile shapes in Figure 5c. This is in line with results from *Lamsal et al.* [2010] who found

closer agreement between OMI DOMINO NO$_2$ and independent data when replacing the TM4 with GEOS-CHEM profiles simulated assuming full mixing within the boundary layer. V. Huijnen et al. (Comparison of OMI NO$_2$ tropospheric columns with an ensemble of global and European regional air quality models, manuscript in preparation, 2009) also find larger NO$_2$ concentrations in TM4 in the lowest one to two layers compared to regional air quality models.

[46] The cases in Figure 5 show that using the lidar profile improves the OMI NO$_2$ product toward ground-based observation. When examining these results it is important to consider the spatial mismatch between TM4 (3° by 2°) and the lidar observations at one location in the Netherlands. With this study we provide an investigation of how well TM4 is able to produce reasonable NO$_2$ profile shapes for 9 days in September. For some cases the TM4 a priori profile appears reasonable but for other cases the TM4 a priori profile is not a good estimate of the actual NO$_2$ profile. The reasonable agreement in profile shape between lidar and TM4 may occur because conditions at Cabauw were such that the observed NO$_2$ profile was representative of a regional profile.

[47] We investigated the effects of the lidar 10% systematic error on the resulting improved AMF. We found that improved AMFs changed by less than 3% when lidar profiles were increased by 10%. We also investigated the effect of accounting for free tropospheric NO$_2$. We added TM4 free tropospheric NO$_2$ to the lidar and MoO-CL observations and for the cleaner day, 9 September, the average of the ground-based observations increased by 9% with this addition. For the more polluted day, 12 September, adding free tropospheric NO$_2$ from TM4 increased the average of the ground-based observations by 5%. For both cases adding free tropospheric NO$_2$ from TM4 brought OMI and ground-based observations in closer agreement.

4.2.2. Southeastern Pollution: Comparison of NO$_2$ Profiles and AMFs

[48] Figure 6 shows NO$_2$ profiles for flights over the southeastern United States and the Gulf of Mexico on 4 March 2006. The pressure level where the lowest LIF/DC-8 measurement was made is indicated. All values below this (gray dashed line) level are estimations determined by extrapolating the median of the lowest 10 NO$_2$ mixing ratio observations to the surface. The first flight segment over Mississippi and Alabama observed values of NO$_2$ near the surface with peaks of 3.5 μg m^{-3} (1 ppb). The second flight segment over the Gulf of Mexico also observed enhanced NO$_2$ at 500 m, though the peak NO$_2$ values were less than 0.8 μg m^{-3} (0.5 ppb). The OMI ground pixels overlapping these profiles showed enhanced NO$_2$ in the Mississippi and Alabama areas and outflow of NO$_2$ into the Gulf of Mexico. For the flight segment made over Mississippi and Alabama, Figure 6a shows that TM4 estimates the NO$_2$ higher in the planetary boundary layer than the LIF/DC-8 observes (the LIF/DC-8 observes an NO$_2$ peak at 950 hPa). TM4 also estimates less NO$_2$ in the free troposphere than the LIF/DC-8 observes. The improved AMF is 20% larger than the original and the improved OMI is 20% smaller than original OMI. For this comparison, using the improved AMF improves the agreement between OMI and LIF/DC-8. In this case 29% of the LIF/DC-8 profile was extrapolated to the surface.
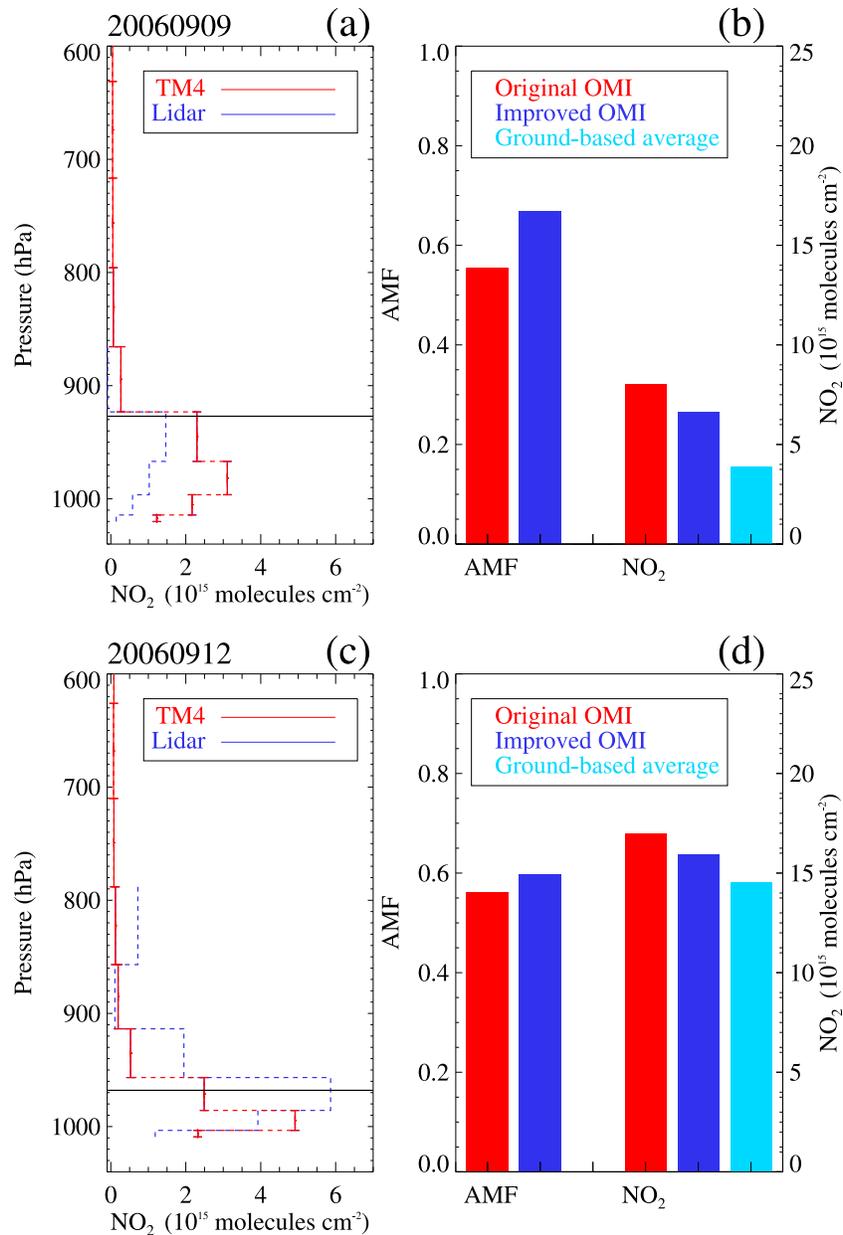
Figure 5. The partial tropospheric NO$_2$ column content from the TM4 (red) and the lidar (blue) for (a and b) 9 September and (c and d) 12 September 2006. The plots are labeled with the YYYYMMDD date format. In Figures 5a and 5c the vertical error bars show the pressure range over which the column content extends. The dashed lines are drawn as a guide to the eye. The boundary layer height is shown in black. Figures 5b and 5d show the original (red) and improved (blue) AMF as well as the original (red) and improved (blue) OMI NO$_2$ columns. The ground-based average NO$_2$ column is shown in light blue. The ground-based average NO$_2$ column is the average of the three MAXDOAS instruments, the lidar, and the MoO-CL observations.

[49] For the flight segment in the Gulf of Mexico (Figures 6c and 6d) OMI observes much more NO$_2$ than measured by the LIF/DC-8. The average OMI cloud radiance fraction for this day is 0.3 and clouds can have the effect of masking or enhancing NO$_2$, depending on the vertical distribution of NO$_2$ with respect to cloud height. For this case, the average OMI cloud height was 840 hPa, and it is possible that clouds had the effect of enhancing NO$_2$. The aircraft profile was made 3 h after the OMI overpass and changes in wind and chemistry may also explain the differences between OMI and the LIF/DC-8 NO$_2$. Figure 6c shows the NO$_2$ partial columns from LIF/DC-8 and TM4 for the flight segment off the coast of Texas, in the Gulf of Mexico. Here TM4 simulates a stronger NO$_2$ peak in the planetary boundary layer than observed by the LIF/DC-8. The improved AMF is 33% larger than the original but there is considerable uncertainty in this change because 25% of the LIF/DC-8 NO$_2$ profile was based on extrapolation. The improved OMI is closer to
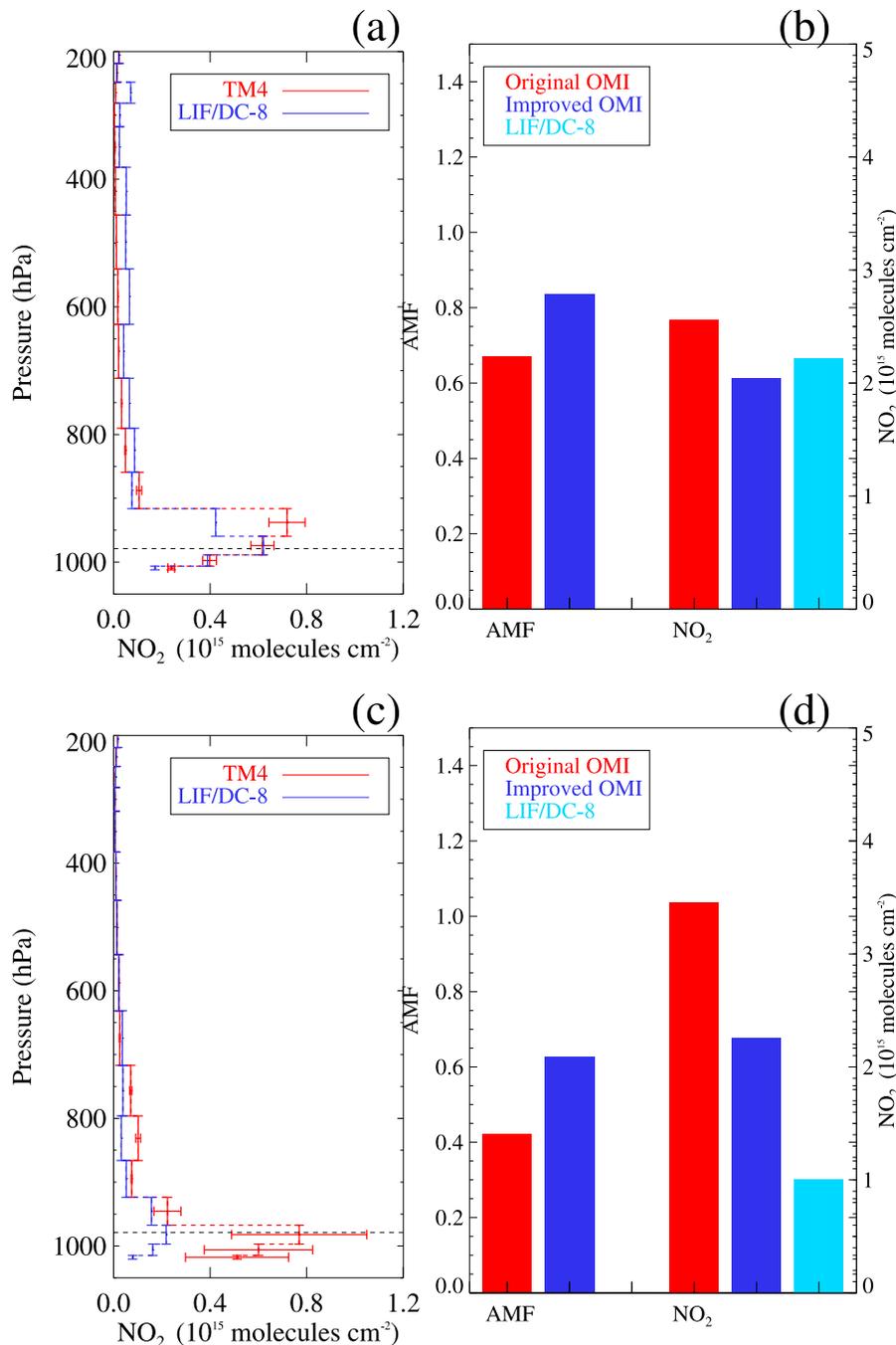
Figure 6. Partial tropospheric NO₂ columns for TM4 (red) and LIF/DC-8 (blue) for 4 March 2006 for flight segments over (a and b) Mississippi and Alabama and (c and d) the Gulf of Mexico. In Figures 6a and 6c the vertical error bars show the pressure range over which the column content extends. Typically, more than one OMI ground pixel overlapped an LIF/DC-8 profile, and there is more than one TM4 profile corresponding with the LIF/DC-8 profile. Horizontal error bars show the standard deviation of the TM4 values. The horizontal gray dashed line shows where the lowest LIF/DC-8 measurement was made. All LIF/DC-8 measurements below this were estimated using extrapolation. Figures 6b and 6d show the original (red) and improved (blue) AMF, the original and improved OMI NO₂ columns, and the LIF/DC-8 integrated NO₂ (light blue).

the LIF/DC-8 measurement, though improved OMI is still 2.3 times larger than the LIF/DC-8 column. In section 4.2.4 we will show that on average using the observed profiles improves the OMI NO₂ retrieval.

4.2.3. Terrain Height Effects on AMF

[50] Figure 7 shows TM4 and LIF/DC-8 profiles as well as OMI and LIF/DC-8 NO₂ column contents for flight segments made over Mexico City on 11, 16 and 19 March
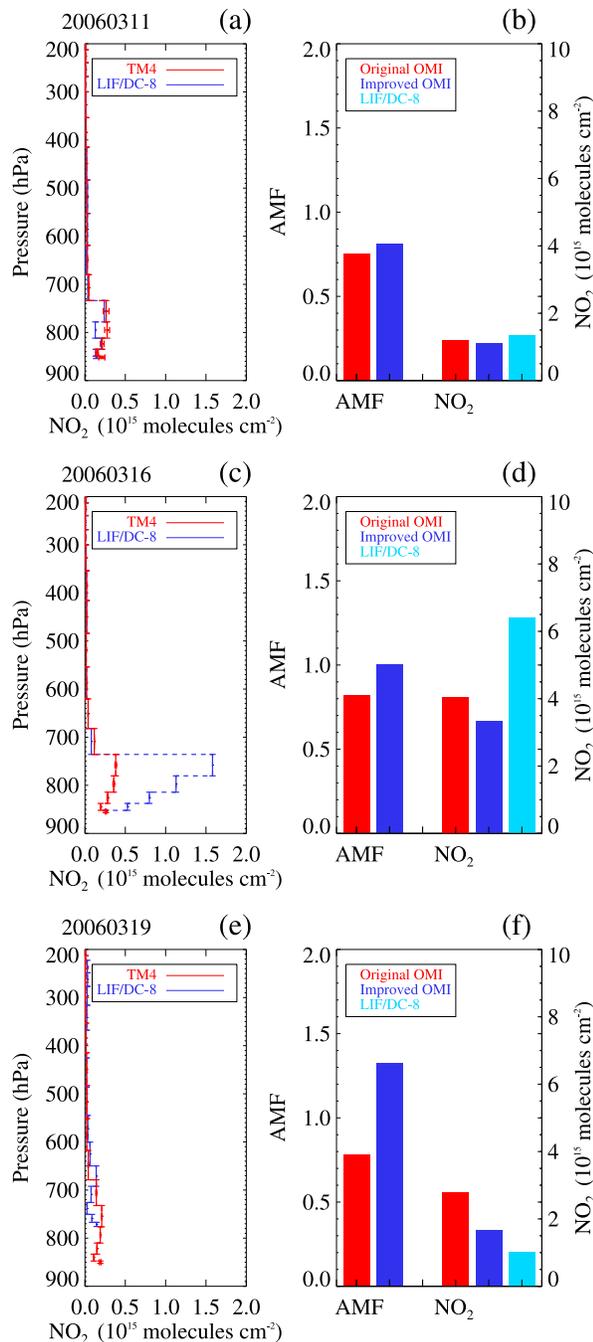
Figure 7. Partial tropospheric NO$_2$ columns from the TM4 model (red) and the LIF/DC-8 (blue) for flights near Mexico City on (a and b) 11 March, (c and d) 16 March, and (e and f) 19 March 2006. The plots are labeled with the YYYYMMDD date format. In Figures 7a, 7c, and 7e the vertical error bars show the pressure range over which the column content extends. Typically, more than one OMI ground pixel overlapped an LIF/DC-8 profile, and there is more than one TM4 profile corresponding with the LIF/DC-8 profile. Horizontal error bars show the standard deviation of the TM4 values. Figures 7b, 7d, and 7f show the original (red) and improved (blue) AMF, the original and improved OMI NO$_2$ columns, and the LIF/DC-8 integrated NO$_2$ (light blue).

2006. For 11 March, the TM4 profile is similar to the profile measured by the LIF/DC-8 and changes to the improved AMF and OMI NO$_2$ are small (Figures 7a and 7b). This flight included a transect through the boundary layer and the portion of the column extrapolated to the surface accounted for 55% of the total column.

[51] For 16 March the LIF/DC-8 profile shows more NO$_2$ near the top of the boundary layer than the TM4 profile. These differences result in increasing the AMF and decreasing the improved NO$_2$ (Figures 7c and 7d). For this case using the LIF/DC-8 profile does not bring the OMI NO$_2$ closer to the observed column. This profile like the profile on 11 March included a transect through the boundary layer and the portion of the column extrapolated to the surface accounted for 51% of the total column. The TM4 profile shape for 11 March was similar to that measured by the LIF and the OMI NO$_2$ did not change much when we incorporated the measured profile. The measured profile for 16 March was very different from the TM4 profile and may be more representative of local pollution that TM4 cannot capture. The flights on 11 and 16 March were made to the south of Mexico City and measured outflow from the city. This outflow is difficult to capture with the coarse resolution TM4 model.
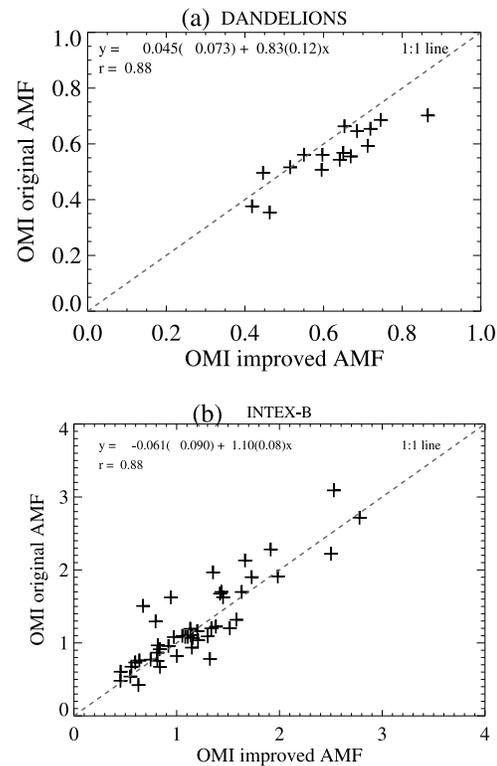
Figure 8. Comparisons of original and improved air mass factors for (a) DANDELIONS and (b) INTEX-B campaigns. For the DANDELIONS campaign, the improved air mass factors were mostly larger than the original values. The improved AMFs for the INTEX-B campaign were determined with measured LIF/DC-8 NO$_2$ profiles, and for Mexico City the improved AMFs were determined with the LIF/DC-8 profiles and improved estimates of surface pressure. The 1:1 line is shown with a dashed line.

Table 4. Slope and Correlation Coefficient for Comparisons Among Original OMI NO$_2$ and DANDELIONS Ground-Based Average NO$_2$, Improved OMI NO$_2$ and DANDELIONS Ground-Based Average NO$_2$, Original OMI NO$_2$ and INTEX-B LIF/DC-8 NO$_2$, and Improved OMI NO$_2$ and INTEX-B LIF/DC-8 NO$_2$

y Axis	x Axis	Slope	Correlation Coefficient (r)	Number of Observations
Original OMI NO$_2$	DANDELIONS ground-based average NO$_2$	1.07 ± 0.37	0.77	16
Improved OMI NO$_2$	DANDELIONS ground-based average NO$_2$	0.97 ± 0.30	0.77	16
Original OMI NO$_2$	INTEX-B LIF/DC-8 NO$_2$	0.87 ± 0.29	0.74	46
Improved OMI NO$_2$ (shape changes only)[a]	INTEX-B LIF/DC-8 NO$_2$	0.88 ± 0.12	0.79	46

[a]The improved OMI NO$_2$ for INTEX-B cases also involve changes in surface pressure.

[52] The 19 March profile was made over Mexico City (18.9° latitude −99.0° longitude) and the TM4 surface pressure grid is too coarse to capture the variation in terrain height over this area. For all three cases near Mexico City we recalculated the AMFs using the high-resolution terrain heights from the OMI product. Figure 7e shows that for 19 March the high-resolution terrain heights of 780 hPa were much smaller than the TM4 terrain heights of 860 hPa. This change in terrain height had the effect of increasing the AMF and decreasing the OMI NO$_2$ which brought the improved OMI NO$_2$ closer to the LIF/DC-8 column. Similar retrieval improvements have been reported by *Zhou et al.* [2009].

4.2.4. Comparisons of Original and Improved AMFs

[53] Figure 8 shows a comparison between the original and improved AMFs for the DANDELIONS and INTEX-B campaigns. The improved AMFs include only changes in profile shape except for the three flights around Mexico City where the surface pressures were also changed because TM4 could not capture the highly variable terrain height. For the DANDELIONS campaign the improved AMF is generally larger than the original, likely because of insufficient boundary layer mixing in TM4 over the Netherlands, and the slope (original/improved) is 0.83. Table 4 shows the statistics for comparisons among DANDELIONS average ground-based NO$_2$ and improved OMI and original OMI. The slopes are between 0.97 and 1.07 and the correlation coefficients are 0.77. The slope and correlation coefficient for the improved OMI and DANDELIONS NO$_2$ are less than 10% different from the statistics for the original OMI and DANDELIONS NO$_2$.

[54] For INTEX-B the improved AMF is similar to the original with a slope (original/improved) of 1.10 (Figure 8b). In Figure 8b three points over Mexico City include changes to the profile shape and surface height. Table 4 shows that the correlation coefficient for the improved OMI and LIF/DC-8 tropospheric NO$_2$ is 0.79, better than that for the original OMI and LIF/DC-8 NO$_2$, where r = 0.74. The slope comparing the original OMI and LIF/DC-8 NO$_2$ is 0.87 ± 0.29 (2 standard deviations) and the slope comparing improved OMI and LIF/DC-8 NO$_2$ is 0.88 ± 0.12.

[55] Another way to compare the measurements is by averaging NO$_2$ columns as shown in Figure 9 for the different regions examined. For DANDELIONS TM4 profile
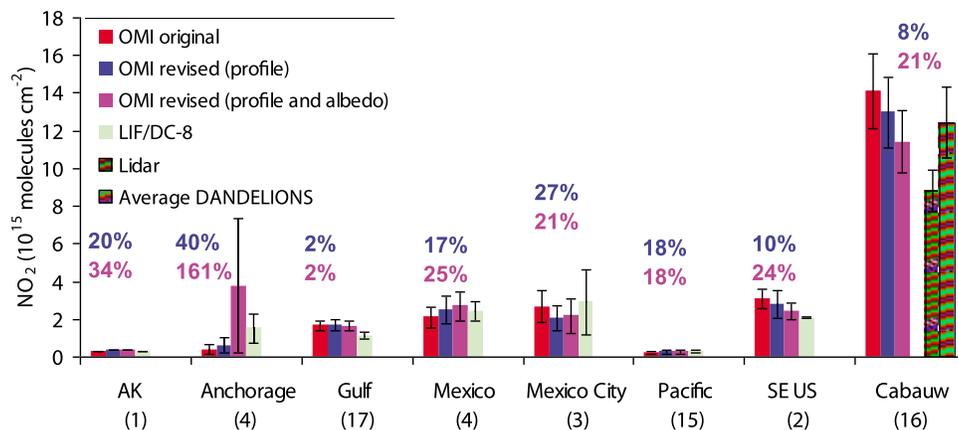
Figure 9. Average original and improved NO$_2$ from OMI, INTEX-LIF/DC-8, and lidar and the average of all ground-based observations from DANDELIONS (Average DANDELIONS). See the legend for color denotations of the various data products. The improved OMI NO$_2$ over Mexico City includes changes to the profile shape and the surface pressure. The error bars show the standard deviation of the mean. The percent difference between original and improved (with respect to profile shape) OMI is written in blue (percent difference = |OMI original − OMI improved|/(OMI original + OMI improved)/2). The percent difference between original and improved (with respect to profile shape and surface albedo) OMI is written in pink. The number of profiles made for each location is shown in parentheses below the location name.

Table 5. Original and Improved Surface Albedo and Original and Improved OMI NO_2 Determined With These Surface Albedos[a]

Location[b]	α_o	α_i	O_o	O_i	Percent Change in Albedo	Percent Change in OMI NO_2 (α_i Only)	Percent Change in OMI NO_2 (Profile Only)	Percent Change in OMI NO_2 (α_i and Profile)
AK (1)	0.14	0.12	0.28	0.32	20	13	20	34
Anchorage (4)	0.23	0.13	0.40	0.42	57	3	40	161
Gulf (17)	0.05	0.05	1.68	1.62	10	4	2	2
Mexico (4)	0.07	0.06	2.10	2.24	11	7	17	25
Mexico City (3)	0.05	0.05	2.67	2.85	5	6	27	21
Pacific (15)	0.08	0.05	0.22	0.21	36	2	18	18
SE U.S. (2)	0.04	0.05	3.08	2.69	24	13	10	24
Cabauw (16)	0.05	0.06	14.1	12.5	18	12	8	21

[a]Also shown is the percent change in surface albedo and the percent change in OMI NO_2 for three cases: (1) accounting for improved surface albedo only, (2) accounting for improved profile only, and (3) accounting for both improved profile and surface albedo. Original and improved surface albedo are α_o and α_i, respectively, and original and improved OMI NO_2 are O_o and O_i, respectively.

[b]The number of flights is written in parentheses next to the location name.

shapes have been improved in the lowest 0–2 km without the need for assumptions in the boundary layer. For INTEX-B, TM4 profiles have been replaced by observations throughout the troposphere but assumptions were needed for the lowest layers of the boundary layer where the aircraft did not sample (below 300 m). Figure 9 shows the number of profiles made in each region and in most regions only a few profiles were made; only a single profile was collected over Alaska. For seven out of the eight regions the original OMI average is within 50% of the field campaign average. For Anchorage, where the original OMI columns are small (0.4 × 10^{15} molecules cm^{-2}) the differences between OMI and field measurements is greater than 50%. For the Netherlands, with the largest average NO_2, the original OMI average is within 10% of the ground-based observations. For important source areas of the Netherlands, the southeastern United States and Mexico, using the measured profile in the algorithm brings improved OMI closer to the field campaign measurement. Figure 9 shows the percent difference between original OMI and improved OMI (O_o and O_i), where percent difference is calculated with the following:

$$D = \frac{|O_o - O_i|}{(O_o + O_i)/2}. \qquad (3)$$

[56] For the eight cases the percent difference between original and improved OMI ranged from 2 to 40% and this represents the sensitivity of OMI NO_2 to profile shape estimates. Figure 9 also shows the standard deviation of the mean for each case and the changes between the original and improved OMI do not exceed the standard deviation of the mean. The large values for the standard deviation of the mean are from the variability and the limited number of measurements for each group. Another consideration for the INTEX-B cases is the effects of the extrapolation of the profile, which introduces uncertainties in the AMF and the improved OMI. The absolute average change in OMI NO_2 related to profile shapes estimates is 15% with a standard deviation of 14% and this is comparable to previous studies [Martin et al., 2004, 2006; Schaub et al., 2006; Bucsela et al., 2008] although these studies used different retrievals, different models (GEOS-CHEM, TM3, TM4), different model sampling (daily, annual average) and different observational data sets (see Table 1).

4.3. Influence of Surface Albedo on AMFs

[57] We examined the effects of using improved surface albedo maps in the OMI retrieval. Table 5 shows the original and improved surface albedos [Kleipool et al., 2008] as well as OMI NO_2, derived with the original and improved surface albedos. Table 5 shows that when the surface albedo increases OMI NO_2 decreases. When the surface albedo increases, OMI is generally more sensitive to NO_2 and the AMF increases, resulting in smaller retrieved NO_2 tropospheric columns. Table 5 shows that albedo changes are most important in polluted situations with low albedos, illustrated by the largest (13%) decrease in OMI NO_2 for the southeastern United States where the albedo is relatively small. These changes in OMI NO_2 are related to changes in surface albedo only. We address changes in both surface albedo and profile shape below.

[58] Figure 9 shows improved OMI retrieved with AMFs that use a combination of the Kleipool et al. [2008] surface albedo maps and LIF/DC-8 and lidar profile shapes. It shows that accounting for all of these factors results in OMI NO_2 changes ranging from 2% to 34%, excluding Anchorage. The largest change, of 161% occurred over Anchorage, Alaska, where the improved surface albedo was 0.13, half of the original value, and the LIF/DC-8 profile showed large NO_2 values near the surface (Figure 4). Both of these factors resulted in reducing the AMF and thus increasing the OMI NO_2; this increase is nonlinear. The results from changing both profile shape and surface albedo show that the inaccuracies in surface albedo have larger impacts on areas where surface albedos are relatively large and where there are significant levels of NO_2 near the surface. The absolute average change in OMI NO_2 related to profile shapes estimates and surface albedo estimates is 23% with a standard deviation of 27%. Figure 9 shows that improving both the NO_2 profile shape and the surface albedo improves the agreement between OMI and field observations in the Gulf of Mexico, Mexico, the southeastern United States and the Netherlands.

[59] On average using the lidar and LIF/DC-8 profiles in the algorithm improves the OMI retrieval. There were some cases like those over Mexico City and Anchorage (Figure 9) where using the observed profiles did not improve agreement. These cases are the most difficult to improve because

they suffered more from additional uncertainties in the estimate of the terrain height (Mexico City) and in albedo which for Anchorage decreased from 0.23 to 0.13 from the original and improved surface albedo maps. These cases were also strongly influenced by representativeness issues such as strong horizontal gradients that exist near Mexico City.

5. Conclusions

[60] We used extensive profile and column NO_2 measurements over the Netherlands during the DANDELIONS campaign (September 2006) and over North America during the INTEX-B mission (spring 2006) to quantify errors and suggest improvements for OMI NO_2 retrievals. Previous studies focused on single-campaign validation of OMI tropospheric NO_2, making it difficult to draw general conclusions on the OMI data quality. Here we combine valuable information from the INTEX-B and DANDELIONS campaigns to establish the most comprehensive validation set to date, and interpret our validation results in the context of observed NO_2 profiles as well as improved estimates of surface albedo and terrain height.

[61] We validated tropospheric NO_2 columns from the Dutch OMI NO_2 (DOMINO) algorithm, and the OMI standard product algorithm based on improved Collection 3 data with four different ground-based techniques during DANDELIONS and from an aircraft during INTEX-B. More than 60 coincident measurements were found, providing an excellent opportunity to validate the OMI NO_2 products over a range of conditions varying from remote marine to highly polluted (Mexico City and the Netherlands). We find that for both campaigns DOMINO compares well ($r > 0.74$, no significant bias) with ground-based and in situ columns of NO_2. The standard product generally shows less scatter than DOMINO, but is biased low by 40% during INTEX-B. These results are an in line with previous studies [*Boersma et al.*, 2008; *Brinksma et al.*, 2008; *Bucsela et al.*, 2008].

[62] The air mass factor defines the relationship between the measured radiances and NO_2 vertical columns and is the primary source of error in NO_2 satellite retrievals for areas with enhanced NO_2. The standard approach for computing the air mass factor is to use local vertical profile information from a chemical transport model, and for this work TM4 was used for the DOMINO product. We used the observed vertical profiles of NO_2 to evaluate the capability of TM4 to accurately simulate vertical distributions of NO_2 at the spatial scale of an OMI footprint. On average, TM4 profiles compare reasonably well with the observations. Over the Netherlands, we find evidence that TM4 mixing of NO_2 is too weak in the boundary layer. This finding could not be confirmed with data from INTEX-B, because the aircraft did not sample the lowest part of the atmosphere, where most of the NO_2 resides.

[63] We incorporated the observed vertical profiles of NO_2 into the DOMINO algorithm and we found that observed profiles change OMI retrieved NO_2 on average by 15% (with a standard deviation of 14%). We show case studies related to pollution in the Netherlands and the southeastern United States, and outflow from Mexico City

and the southern United States into the Gulf of Mexico. We replaced the current, surface albedo database with $1° \times 1°$ spatial resolution, with the recent *Kleipool et al.* [2008] OMI albedo set with $0.5° \times 0.5°$ spatial resolution, and found changes in OMI tropospheric NO_2 of up to 13%, with the strongest effect in polluted situations over dark terrain. The average change in OMI tropospheric NO_2 related to combined changes in profile and surface albedo estimates is 23% with a standard deviation of 27%, and brings the retrievals into better agreement with the validation set.

[64] The quality of the DOMINO product shown here provides some confidence in using the data for air quality applications and for top-down constraints on NO_x emissions. This work recommends the implementation of the new albedo set by *Kleipool et al.* [2008] in OMI retrievals. Future work should focus on also using other forward model parameters including a priori profile shapes and surface pressures with spatial resolution similar to the satellite footprint. Aerosols likely impact air mass factors for satellite and ground-based DOAS retrievals. The CINDI (CABOW Intercomparison of Nitrogen Dioxide Instruments) campaign at Cabauw in summer 2009 (http://www.knmi.nl/samenw/cindi/) will be particularly important in examining this issue further as it will bring together a suite of instruments with very different sensitivities to aerosols as well as aerosol instrumentation.

References

Acarreta, J. R., J. F. De Haan, and P. Stammes (2004), Cloud pressure retrieval using the O_2-O_2 absorption band at 477 nm, *J. Geophys. Res.*, *109*, D05204, doi:10.1029/2003JD003915.

Apituley, A., A. van Lammeren, and H. Russchenberg (2000), High time resolution cloud measurements with lidar during CLARA, *Phys. Chem. Earth, Part B*, *25*, 107–113, doi:10.1016/S1464-1909(99)00135-5.

Blond, N., K. F. Boersma, H. J. Eskes, R. J. van der A, M. Van Roozendael, I. De Smedt, G. Bergametti, and R. Vautard (2007), Intercomparison of SCIAMACHY nitrogen dioxide observations, in situ measurements, and air quality modeling results over western Europe, *J. Geophys. Res.*, *112*, D10311, doi:10.1029/2006JD007277.

Boersma, K. F., H. J. Eskes, and E. J. Brinksma (2004), Error analysis for tropospheric NO_2 retrieval from space, *J. Geophys. Res.*, *109*, D04311, doi:10.1029/2003JD003962.

Boersma, K. F., et al. (2007), Near-real time retrieval of tropospheric NO_2 from OMI, *Atmos. Chem. Phys.*, *7*, 2103–2118.

Boersma, K. F., et al. (2008), Validation of OMI tropospheric NO$_2$ observations during INTEX-B and application to constrain NO$_x$ emissions over the eastern United States and Mexico, *Atmos. Environ.*, *42*(19), 4480–4497, doi:10.1016/j.atmosenv.2008.02.004.

Boersma, K. F., D. J. Jacob, M. Trainic, Y. Rudich, I. DeSmedt, R. Dirksen, and H. J. Eskes (2009), Validation of urban NO$_2$ concentrations and their diurnal and seasonal variations observed from space (SCIAMACHY and OMI sensors) using in situ measurements in Israeli cities, *Atmos. Chem. Phys.*, *9*, 3867–3879.

Brinksma, E. J., et al. (2008), The 2005 and 2006 DANDELIONS NO$_2$ and aerosol intercomparison campaigns, *J. Geophys. Res.*, *113*, D16S46, doi:10.1029/2007JD008808.

Bucsela, E. J., E. Celarier, M. Wenig, J. Gleason, P. Veefkind, K. F. Boersma, and E. Brinksma (2006), Algorithm for NO$_2$ vertical column retrieval from the Ozone Monitoring Instrument, *IEEE Trans. Geosci. Remote Sens.*, *44*, 1245–1258.

Bucsela, E. J., et al. (2008), Comparison of tropospheric NO$_2$ from in situ aircraft measurements with near-real-time and standard product data from OMI, *J. Geophys. Res.*, *113*, D16S31, doi:10.1029/2007JD008838.

Celarier, E. A., et al. (2008), Validation of Ozone Monitoring Instrument nitrogen dioxide columns, *J. Geophys. Res.*, *113*, D15S15, doi:10.1029/2007JD008908.

Clarke, M. R. B. (1980), The reduced major axis of a bivariate sample, *Biometrica*, *67*(2), 441–446, doi:10.1093/biomet/67.2.441.

Day, D. A., P. J. Wooldridge, M. B. Dillon, J. A. Thornton, and R. C. Cohen (2002), A thermal dissociation laser-induced fluorescence instrument for in situ detection of NO$_2$, peroxy nitrates, alkyl nitrates, and HNO$_3$, *J. Geophys. Res.*, *107*(D6), 4046, doi:10.1029/2001JD000779.

Dobber, M., Q. Kleipool, R. Dirksen, P. Levelt, G. Jaross, S. Taylor, T. Kelly, L. Flynn, G. Leppelmeier, and N. Rozemeijer (2008a), Validation of Ozone Monitoring Instrument level 1b data products, *J. Geophys. Res.*, *113*, D15S06, doi:10.1029/2007JD008665.

Dobber, M. R., R. Voors, R. Dirksen, Q. Kleipool, and P. Levelt (2008b), The high-resolution solar reference spectrum between 250 and 550 nm and its application to measurements with the Ozone Monitoring Instrument, *Sol. Phys.*, *249*, 281–291, doi:10.1007/s11207-008-9187-7.

Dunlea, E. J., et al. (2007), Evolution of nitrogen dioxide chemiluminescence monitors in a polluted urban environment, *Atmos. Chem. Phys.*, *7*, 2691–2704.

Fehsenfeld, F. C., et al. (1990), Intercomparison of NO$_2$ measurement techniques, *J. Geophys. Res.*, *95*(D4), 3579–3597, doi:10.1029/JD095iD04p03579.

Heland, J., H. Schlager, A. Richter, and J. P. Burrows (2002), First comparison of tropospheric NO$_2$ column densities retrieved from GOME measurements and in situ aircraft profile measurements, *Geophys. Res. Lett.*, *29*(20), 1983, doi:10.1029/2002GL015528.

Hudman, R. C., et al. (2007), Surface and lightning sources of nitrogen oxides over the United States: Magnitudes, chemical evolution, and outflow, *J. Geophys. Res.*, *112*, D12S05, doi:10.1029/2006JD007912.

Irie, H., Y. Kanaya, H. Akimoto, H. Tanimoto, Z. Wang, J. F. Gleason, and E. J. Bucsela (2008), Validation of OMI tropospheric NO$_2$ column data using MAXDOAS measurements deep inside the North China Plain in June 2006: Mount Tai Experiment 2006, *Atmos. Chem. Phys.*, *8*, 6577–6586.

Jaeglé, L., R. V. Martin, K. Chance, L. Steinberger, T. P. Kurosu, D. J. Jacob, A. I. Modi, V. Yoboué, L. Sigha-Nkamdjou, and C. Galy Lacaux (2004), Satellite mapping of rain-induced nitric oxide emissions from soils, *J. Geophys. Res.*, *109*, D21310, doi:10.1029/2004JD004787.

Kleipool, Q. L., M. R. Dobber, J. F. de Haan, and P. F. Levelt (2008), Earth surface reflectance climatology from 3 years of OMI data, *J. Geophys. Res.*, *113*, D18308, doi:10.1029/2008JD010290.

Koelemeijer, R. B. A., J. F. De Haan, and P. Stammes (2003), A database of spectral surface reflectivity in the range 335–772 nm derived from 5.5 years of GOME observations, *J. Geophys. Res.*, *108*(D2), 4070, doi:10.1029/2002JD002429.

Krol, M., S. Houwwling, B. Bregman, M. van den Broek, A. Segers, P. van Velthove, W. Peters, F. Detener, and P. Bergamaschi (2005), The two-way nested global chemistry-transport zoom model TM5: Algorithm and applications, *Atmos. Chem. Phys.*, *5*, 417–432.

Lamsal, L. N., R. V. Martin, A. van Donkelaar, M. Steinbacher, E. A. Celarier, E. Bucsela, E. J. Dunlea, and J. P. Pinto (2008), Ground-level nitrogen dioxide concentrations inferred from the satellite-borne Ozone Monitoring Instrument, *J. Geophys. Res.*, *113*, D16308, doi:10.1029/2007JD009235.

Lamsal, L. N., R. V. Martin, A. van Donkelaar, E. A. Celarier, R. K. Boersma, R. Dirksen, C. Luo, and Y. Wang (2010), Indirect validation of tropospheric nitrogen dioxide retrieved from the OMI satellite instrument: Insight into the seasonal variation of nitrogen oxides at

northern midlatitudes, *J. Geophys. Res.*, doi:10.1029/2009JD013351, in press.

Levelt, P. F., G. H. J. van den Oord, M. R. Dobber, A. Mälkki, H. Visser, J. de Vries, P. Stammes, J. O. V. Lundell, and H. Saari (2006), The Ozone Monitoring Instrument, *IEEE Trans. Geosci. Remote Sens.*, *44*, 1093–1101, doi:10.1109/TGRS.2006.872333.

Martin, R. V., et al. (2002), An improved retrieval of tropospheric nitrogen dioxide from GOME, *J. Geophys. Res.*, *107*(D20), 4437, doi:10.1029/2001JD001027.

Martin, R. V., D. J. Jacob, K. Chance, T. P. Kurosu, P. I. Palmer, and M. J. Evans (2003), Global inventory of nitrogen oxide emissions constrained by space-based observations of NO$_2$ columns, *J. Geophys. Res.*, *108*(D17), 4537, doi:10.1029/2003JD003453.

Martin, R. V., D. D. Parrish, T. B. Ryerson, D. K. Nicks Jr., K. Chance, T. P. Kurosu, D. J. Jacob, E. D. Sturges, A. Fried, and B. P. Wert (2004), Evaluation of GOME satellite measurements of tropospheric NO$_2$ and HCHO using regional data from aircraft campaigns in the southeastern United States, *J. Geophys. Res.*, *109*, D24307, doi:10.1029/2004JD004869.

Martin, R. V., C. E. Sioris, K. Chance, T. B. Ryerson, T. H. Bertram, P. J. Wooldridge, R. C. Cohen, J. A. Neuman, A. Swanson, and F. M. Flocke (2006), Evaluation of space-based constraints on global nitrogen oxide emissions with regional aircraft measurements over and downwind of eastern North America, *J. Geophys. Res.*, *111*, D15308, doi:10.1029/2005JD006680.

Napelenok, S. L., R. W. Pinder, A. B. Gilliland, and R. V. Martin (2008), A method for evaluating spatially resolved NO$_x$ emissions using Kalman filter inversion, direct sensitivities, and space-based NO$_2$ observations, *Atmos. Chem. Phys.*, *8*, 5603–5614.

Pinardi, G., F. Hendrick, K. Clemer, J. C. Lambert, J. Bai, and M. Van Roozendael (2008), On the use of the MAXDOAS technique for the validation of tropospheric NO$_2$ column measurements from satellite, paper presented at 2008 EUMETSAT Meteorological Satellite Conference, Eur. Org. for the Exploit. of Meteorol. Satell., Darnstadt, Germany.

Schaap, M., A. Apituley, R. M. A. Timmermans, R. B. A. Koelemeijer, and G. de Leeuw (2009), Exploring the relation between aerosol optical depth and PM2.5 at Cabauw, the Netherlands, *Atmos. Chem. Phys.*, *9*, 909–925.

Schaub, D., K. F. Boersma, J. W. Kaiser, A. K. Weiss, D. Folini, H. J. Eskes, and B. Buchmann (2006), Comparison of GOME tropospheric NO$_2$ columns with NO$_2$ profiles deduced from ground-based in situ measurements, *Atmos. Chem. Phys.*, *6*, 3211–3229.

Singh, H. B., W. H. Brune, J. H. Crawford, F. Flocke, and D. J. Jacob (2009), Chemistry and transport of pollution over the Gulf of Mexico and the Pacific: Spring 2006 INTEX-B Campaign overview and first results, *Atmos. Chem. Phys. Discuss.*, *9*, 363–409.

Sneep, M., J. F. de Haan, P. Stammes, P. Wang, C. Vanbauce, J. Joiner, A. P. Vasilkov, and P. F. Levelt (2008), Three-way comparison between OMI and PARASOL cloud pressure products, *J. Geophys. Res.*, *113*, D15S23, doi:10.1029/2007JD008694.

Steinbacher, M., C. Zellweger, B. Schwarzenbach, S. Bugmann, B. Buchmann, C. Ordoñez, A. S. H. Prevot, and C. Hueglin (2007), Nitrogen oxide measurements at rural sites in Switzerland: Bias of conventional measurement techniques, *J. Geophys. Res.*, *112*, D11307, doi:10.1029/2006JD007971.

Thornton, J. A., P. J. Wooldridge, and R. C. Cohen (2000), Atmospheric NO$_2$: In situ laser-induced fluorescence detection at parts per trillion mixing ratios, *Anal. Chem.*, *72*, 528–539, doi:10.1021/ac9908905.

van der A, R. J., H. J. Eskes, K. F. Boersma, T. P. C. van Noije, M. Van Roozendael, I. De Smedt, D. H. M. U. Peters, and E. W. Meijer (2008), Trends, seasonal variability and dominant NO$_x$ source derived from a ten year record of NO$_2$ measured from space, *J. Geophys. Res.*, *113*, D04302, doi:10.1029/2007JD009021.

Volten, H., E. J. Brinksma, A. J. C. Berkhout, J. Hains, J. B. Bergwerff, G. R. Van der Hoff, A. Apituley, R. J. Dirksen, S. Calabretta-Jongen, and D. P. J. Swart (2009), NO$_2$ lidar profile measurements for satellite interpretation and validation, *J. Geophys. Res.*, *114*, D24301, doi:10.1029/2009JD012441.

Wagner, T., B. Dix, C. von Friedeburg, U. Frieß, S. Sanghavi, R. Sinreich, and U. Platt (2004), MAXDOAS O$_4$ measurements: A new technique to derive information on atmospheric aerosols—Principles and information content, *J. Geophys. Res.*, *109*, D22205, doi:10.1029/2004JD004904.

Wagner, T., et al. (2007), Comparison of box-air-mass-factors and radiances for Multiple-Axis Differential Optical Absorption Spectroscopy (MAX-DOAS) geometries calculated from different UV/visible radiative transfer models, *Atmos. Chem. Phys.*, *7*, 1809–1833.

Wittrock, F., H. Oetjen, A. Richter, S. Fietkau, T. Medeke, A. Rozanov, and J. P. Burrows (2004), MAXDOAS measurements of atmospheric

trace gases in Ny-Ålesund—Radiative transfer studies and their application, *Atmos. Chem. Phys.*, 4, 955–966.

Zhou, Y., D. Brunner, K. F. Boersma, R. Dirksen, and P. Wang (2009), An improved tropospheric NO$_2$ retrieval for satellite observations in the vicinity of mountainous terrain, *Atmos. Meas. Tech. Discuss.*, 2, 781–824.

K. F. Boersma, R. J. Dirksen, J. C. Hains, M. Kroon, P. Levelt, and J. P. P. Veefkind, Royal Netherlands Meteorological Institute, Wilhelminalaan 10, De Bilt NL-3732 GK, Netherlands. (jhains@ mde.state.md.us)

E. Bucsela, D. P. J. Swart, and H. Volten, RIVM, Bilthoven, N-3720 BA, Netherlands.

R. C. Cohen and A. E. Perring, Department of Chemistry, University of California, Berkeley, CA 94720, USA.

J. F. Gleason, NASA Goddard Space Flight Center, Code 916, Greenbelt, MD 20771, USA.

O. W. Ibrahim, IUP, University of Heidelberg, D-69120 Heidelberg, Germany.

G. Pinardi and M. van Roozendael, Belgian Institute for Space Aeronomy, Ringlaan-3-Ave. Circulaire, B-1180 Brussels, Belgium.

A. Richter, A. Schoenhardt, and F. Wittrock, Institute of Environmental Physics, University of Bremen, Bremen D-28359, Germany.

T. Wagner, Max-Planck Institute for Chemistry, Universitätscampus, D-55128 Mainz, Germany.